AN ABSTRACT OF THE THESIS OF

Leanna R. Eller for the degree of Master of Science in Radiation Health Physics

presented on November 30, 2010.

Title: An Investigation on Photoneutron Production from Medical Linear Accelerators

Abstract approved:

Kathryn A. Higley

The photoneutron production from three Varian linear accelerators ranging in energies from 6 MV to 23 MV has been investigated. Photoneutrons are produced during (γ, n) interactions with materials located within the treatment head. These unwanted neutrons not only increase patient dose, but may also lead to the requirement of additional shielding for the treatment room. All neutron measurements were made using BD-PND dosimeters manufactured by Bubble Technology Industries. A series of neutron measurements were completed for various geometries and for three IMRT prostate plans. The IMRT plans revealed neutron dose equivalents of 8.92±0.62 uSv/cGy for a 23 MV beam. IMRT was also found to increase the neutron dose to patients by a factor of 1.8 when compared to more conventional radiation therapy plans.

An Investigation on Photoneutron Production from Medical Linear Accelerators

by

Leanna R. Eller

A THESIS

submitted to

Oregon State University

in partial fulfillment of

the requirements for the

degree of

Master of Science

Presented November 30, 2010

Commencement June 2011

Master of Science thesis of Leanna R. Eller presented on November 30, 2010.

APPROVED:

Major Professor, representing Radiation Health Physics

Head of the Department of Nuclear Engineering and Radiation Health Physics

---

Dean of the Graduate School

I understand that my thesis will become part of the permanent collection of Oregon State University libraries. My signature below authorizes release of my thesis to any reader upon request.

Leanna R. Eller, Author

ACKNOWLEDGEMENTS

I would first like to acknowledge my committee members Dr. Eleveld, Dr. Carozza and Dr. Lodwick for taking time out of their busy schedules to serve on my graduate committee. I would also like to thank my advisor, Dr. Kathryn Higley, for her continued dedication to the Health Physics program and its students at Oregon State University. I want to thank my husband, Aaron, and my family for their support and encouragement throughout. And lastly, a special thank you to Russell Gerber for his constant guidance and mentorship during the last few years.

TABLE OF CONTENTS

TABLE OF CONTENTS (Continued)

TABLE OF CONTENTS (Continued)

TABLE OF CONTENTS (Continued)

Page

LIST OF FIGURES

LIST OF FIGURES (Continued)

LIST OF FIGURES (Continued)

LIST OF TABLES

LIST OF TABLES (Continued)

LIST OF TABLES (Continued)

Table | Page

LIST OF TABLES (Continued)

LIST OF TABLES (Continued)

An Investigation on Photoneutron Production from Medical Linear Accelerators

1 INTRODUCTION

Any radiation dose to the patient outside of the intended treatment volume is considered undesirable. There are a number of sources of this added dose. Photon leakage from the treatment head, scattered photons out of treatment volume and photoneutron production all contribute to the excess dose received by patients. The later source, photoneutron production, has been an area of interest for some time, particularly since most modern day linear accelerators are capable of producing photons well above the threshold energy required for a (γ, n) reaction.

There has been much concern that the production of photoneutrons from linear accelerators is substantial enough to pose an elevated health risk to the patient due to the increased dose and unaccounted for biological effects. Neutrons generated from the accelerator also pose potential shielding issues if not accounted for in the initial design and construction of the vault. For these reasons it is important to know the level of photoneutron production produced from the linear accelerator and to understand the proper methods for shielding against these neutrons.

Photoneutrons from medical linear accelerators have been monitored and measured using a variety of techniques, modeling programs, and neutron detectors. The BD-PND (Bubble Detector Personal Neutron Dosimeter) manufactured by Bubble

Technologies[1] is one such detector that is frequently used for neutron monitoring and measurements. It is capable of measuring neutrons in and out of the primary radiation beam and provides immediate dose results.

In the following study BD-PND detectors were used to measure the neutron dose generated from 3 medical linear accelerators for a variety of treatment modalities. Measurements were taken to investigate the variation of neutron dose with field size, both in and outside of primary beam, and increasing depth in water. The BD-PND dosimeters were also used for determining the added neutron dose to patients received during intensity modulated radiation therapy (IMRT) treatments. These measurements provided for a better understanding of the neutron field associated with linear accelerators and the associated patient dose.

[1] Bubble Technology Industries. 31278 Highway 17 Chalk River, Ontario, Canada K0J 1J0, 613-589-2456

2 BACKGROUND

2.1 The Linear Accelerator

A medical linear accelerator uses high-frequency electromagnetic waves to accelerate electrons through a wave guide for the production of high energy electrons and photons. The electron beam can be used for therapy treatment or it can be used for the production of bremsstrahlung photons which are also used for radiotherapy treatment. Linear accelerators, like the one seen in Figure 1, are used daily throughout the world to treat patients.

Figure 1: Varian Trilogy Linear Accelerator

Research and development in external beam radiation therapy was fueled by the invention of the Cobalt machine by H.E. Johns from Canada in the 1950's (1). Shortly after the invention of the Cobalt-60 unit, the medical linear accelerator was developed and hospitals soon began treating patients with this new technology. Early linear accelerators had very limited capabilities in terms of beam modulation, beam energy and patient imaging. However, in the last 50 years the technology surrounding the linear accelerator (linac) has improved vastly. Today's linear accelerators are capable of producing electrons and photons at numerous energies. Many linear accelerators contain on board imaging devices that allow for patient imaging before a treatment for confirmation of tumor position. Modulation of the beam is completed through the use of a series of collimators. And finally, multileaf collimators have been added to shape and modify the beam to allow for a varied intensity across a field and very precise treatment delivery. These are just a few of the many features that modern linear accelerators are capable of offering.

2.1.1 Major Components

A standard medical linear accelerator is composed of several main components. These major components, as seen in Figure 2, are a power supply, modulator, electron gun, microwave power source, accelerating wave guide and treatment head. Each main component is composed of numerous subcomponents; however, the treatment head components will be of primary focus since this is where bremsstrahlung photons are produced and the beam is modulated.

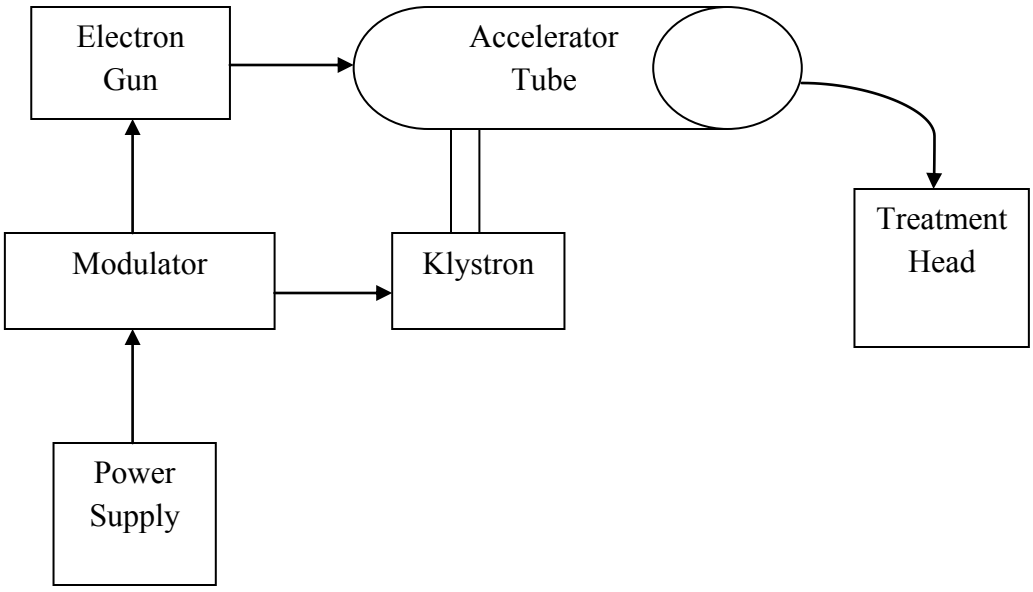

Figure 2: Block diagram of standard medical linear accelerator (Adapted from Khan, 2010)

Electron production begins with the power supply which provides a DC current to the modulator. The modulator provides high powered pulses of only a few microseconds. These negative pulses are sent to the cathode of the klystron and electron gun. The electron gun and klystron simultaneously inject electrons into the accelerator wave guide. The injected electrons have an initial energy of about 50 keV but gain energy through interaction with the electromagnetic field of the microwave (2). The high energy electrons exit the accelerating wave guide as a narrow beam of electrons, about 3 mm in diameter. A bending magnet, used for angling the beam, must be used for accelerators that wish to produce high energy electrons. High energy electron production requires a longer wave guide for acceleration of the electrons. The longer wave guide will not allow for straight-through mounting and requires a system of magnets to change the direction of the electron beam.

Upon entrance of the narrow electron beam into the treatment head it can continue as an electron beam or strike a target for the production of bremsstrahlung photons. The accelerator head contains all the important components for photon production and beam modulation. These components include: retractable x-ray targets, primary and secondary collimators, flattening filters, scattering foils, dual transmission ionization chambers, multileaf collimators, field definition light and an optical distance indicator.

2.1.2 Clinical Electron Production

If the linear accelerator is operated in electron mode the x-ray target and flattening filter will be retracted, and the electron beam will pass through without interaction as shown in Figure 3. A scattering foil made of a high Z material, such as lead, is used to scatter the narrow 3 mm electron beam. The beam will strike the thin foil and scatter. The lead is designed to be thin enough to minimize bremsstrahlung radiation; however, some electrons will interact and appear as x-ray contamination of the electron beam (2). Collimation of the electron beam is achieved using various electron applicators. Since electrons scatter readily in air, the beam collimation must be achieved close to the skin surface of the patient (2). Electron applicators are attached to the treatment head as shown in Figure 3. A lead or Cerrobend cutout is used to provide field shaping at the end of the electron applicator. Cerrobend is an alloy of bismuth, lead, tin and cadmium. It is advantageous over lead due to the lower melting temperature and its ability to be shaped and molded more easily.

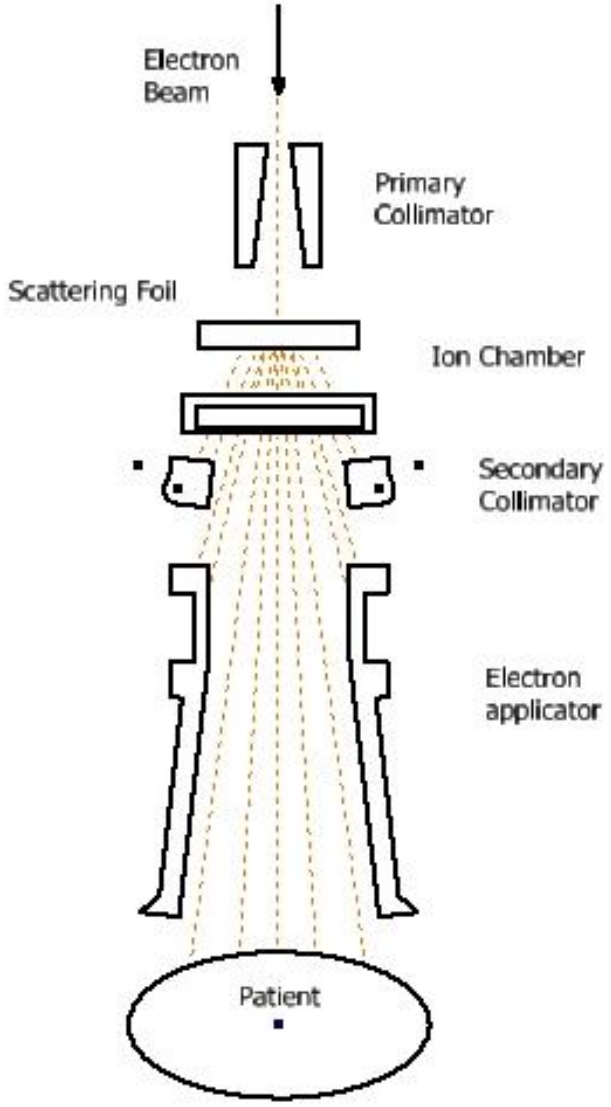

Figure 3: Components of treatment head – Electron Therapy Mode (Adapted from Khan, 2010)

2.1.3 Clinical Photon Production

Clinical photon beams are produced through the use of an x-ray target as shown in Figure 4. A high Z material, such as tungsten, is typically used as the target;

however materials such as lead or lead-tungsten alloys have also been used (2). The electron beam strikes the target and undergoes a series of bremsstrahlung type interactions before losing all kinetic energy within the target. A bremsstrahlung interaction occurs when a high speed electron passes by a nucleus, and due to the Coulomb forces, undergoes deflection and acceleration. The sudden change in direction of the electron causes some of its energy to be released in the form of electromagnetic radiation. The target is designed to be thick enough to reduce the number of electrons that traverse the target without interacting and thin enough to minimize attenuation of photons.

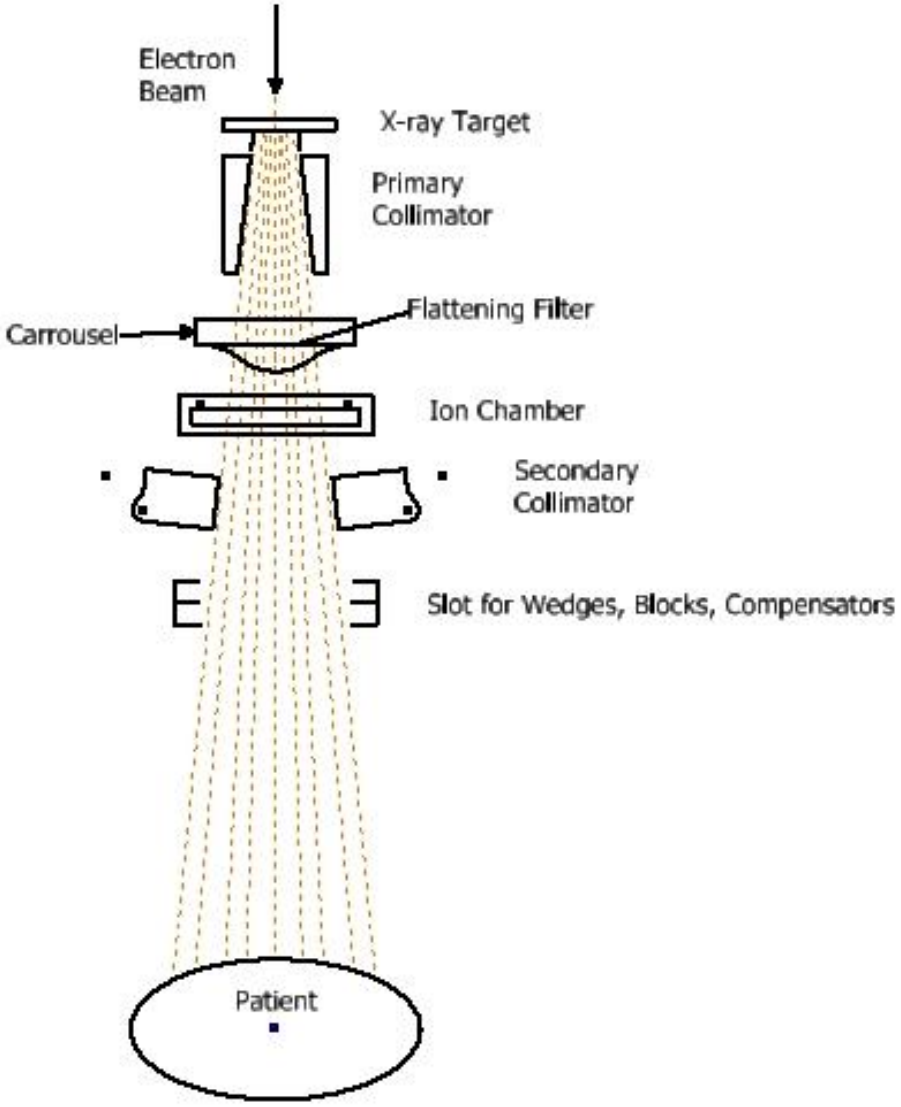

Figure 4: Components of treatment head - X-Ray therapy mode (Adapted from Khan, 2010)

The x-rays beam generated in the target will undergo collimation through a set of collimators. A standard linear accelerator consists of both primary and secondary collimators. The primary collimator defines the maximum circular field, which is then further truncated with the use of an adjustable rectangular collimator (1). The secondary collimators consist of two pairs of jaws that can produce rectangular field sizes, ranging in size from zero to a maximum field size of 40 cm x 40 cm at 100 cm SSD. Once the x-ray beam exits the primary collimators it will pass through a flattening filter. X-rays produced in the target have a forward peaked intensity; therefore, flattening filters are used to create a uniform dose profile across the beam. Flattening filters are typically composed of lead, copper or steel and are conical in structure.

As the beam exits the flattening filter it will approach the ion chambers. The ion chambers monitor dose rate, symmetry and integrated dose. After passing through the chambers, the photon beam will be collimated by the secondary collimators, and if desired, by the multileaf collimator. A multileaf collimator, commonly referred to as an MLC, is used to shape and modulate the radiation beam. The Millennium™ MLC, seen in Figure 5, was created by Varian and includes 120 MLC leaves with inner leaves of 5 mm width and outer leaves of 10 mm width. The increased number of leaves improves the precision and accuracy for the treatment, particularly for smaller lesions.

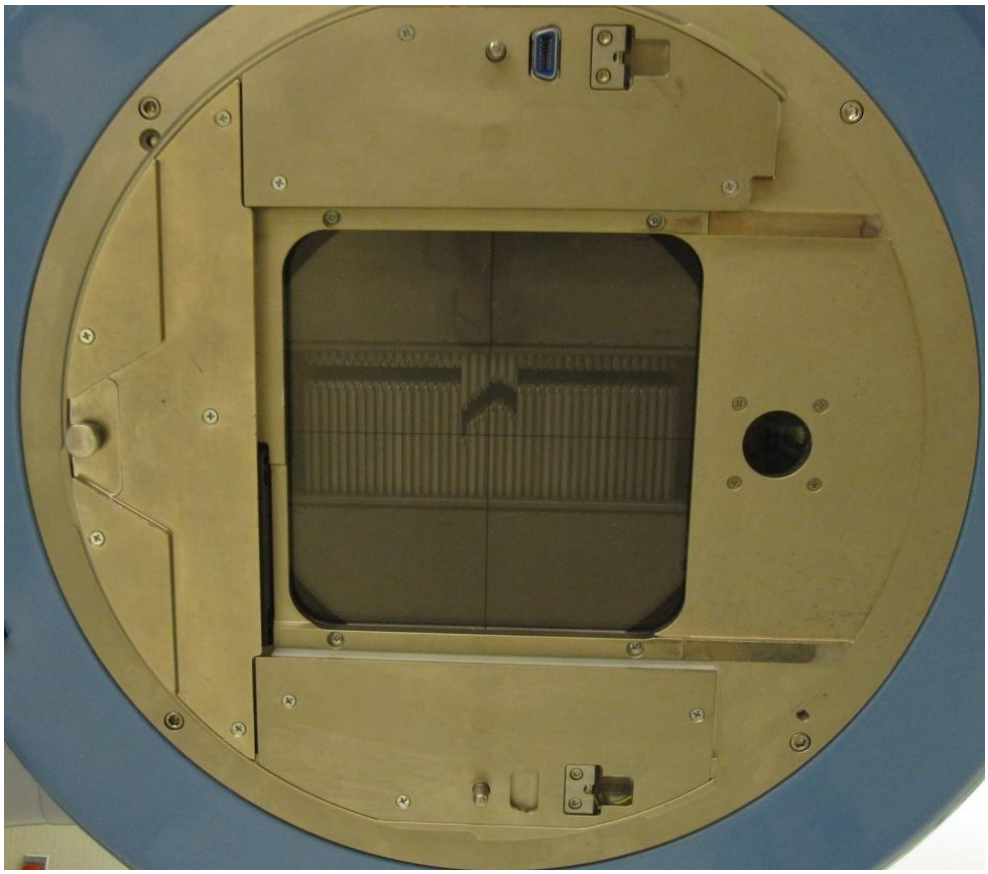

Figure 5: Varian Millennium™ MLC

2.2 Fundamental Interactions

2.2.1 Photon Interactions

There are a number of ways in which photons can interact with matter; however, the three main interactions are photoelectric absorption, Compton scattering and pair production. The specific type of photon interaction that occurs is dependent on the energy of the incident photon and also the atomic number Z of the absorber. The photoelectric effect is dominant for photons below an energy of about 0.1 MeV,

whereas pair production dominates for energies above 5.0 MeV. Compton scattering is the most prominent in the region between photoelectric and pair production interactions and is the primary interaction in energies associated with radiation therapy.

The photoelectric effect occurs when a photon interacts with an atom and ejects an orbital electron of the target atom. The ejected electron, commonly referred to as the photoelectron, has an associated energy equal to that of the incident photon energy minus the electrons associated binding energy. The photoelectric effect is dominant for low-energy photons and high-atomic-numbered absorbers.

Compton scattering involves the collision of a photon with a nearly free electron. The incident photon collides with the electron, which is assumed to be at rest, and transfers some of its energy and momentum. The electron is set in motion and unlike photoelectron absorption, the photon is not absorbed, but instead scattered with a reduced energy.

The third main interaction is pair production which occurs when a photon, with energy greater than 1.02 MeV, interacts with the strong electromagnetic field of an atom. The photons energy will be used in the creation of an electron/positron pair. The electron/positron pair will have a rest mass of 0.511 MeV each. Therefore, the incident photon's energy must exceed 1.02 MeV for pair production to occur.

2.2.2 Neutron Interactions

Neutron interactions are heavily dependent on neutron energy; as a result the classification of neutrons is based on their energy. Fast neutrons are those with energy above 100 keV, slow neutrons have an energy of approximately 1 keV, epithermal neutrons are around 1 eV and thermal neutrons have an energy less than 0.025 eV. Neutron interactions, unlike photons interactions, occur primarily with atomic nuclei. Although neutron-electron interactions do occur, this type of interaction is highly unlikely and considered insignificant when compared to neutron interactions with the nucleus (3). Neutron interactions can be separated into two categories: scattering and absorption. Scattering interactions consist of elastic and inelastic scattering. Absorption interactions consist of electromagnetic, charged, neutral and fission interactions.

As a beam of neutrons travels through bulk matter, the intensity of the beam will decrease as neutrons are removed through nuclear reactions (4). The intensity of the beam will decrease exponentially as shown in Equation 1. The microscopic cross section of the absorbing material, σ, multiplied by the number of atoms per cm^3 for the absorbing material, N, results in the macroscopic cross section designated as Σ. The macroscopic cross section is the inverse of the mean free path, λ. The mean free path is the average distance a neutron will travel in a material between two collisions.

$$I = I_0 e^{-\sigma N t} \qquad \textbf{(Equation 1)}$$

High energy neutrons must undergo many scattering interactions before there is a high probability of absorption. Elastic and inelastic scattering events help to moderate the fast neutrons to energies at which absorption can occur. Inelastic scattering occurs when a neutron interacts with a nucleus leaving it in an excited state and then scatters off with a kinetic energy less than that of its incident energy. The excited nucleus will release its excitation energy in the form of a photon. Typically the cross section for inelastic scattering is small for lower energy, fast neutrons (5).

Elastic scattering is the most probable interaction between fast neutrons and low atomic-number absorbers (5). This interaction conserves both kinetic energy and momentum. The amount of energy transferred per collision is dependent upon the atomic mass of the absorber. From Equation 2, it is evident that a low mass number absorber will allow for more energy transfer per collision than an absorber with a high mass number. This energy loss will slow the neutron and allow for the capture of the neutron by a nucleus.

$$E = E_0 \left(\frac{M-m}{M+m}\right)^2 \qquad \textbf{(Equation 2)}$$

Absorption occurs when a neutron is moderated to energies low enough to be captured by a nucleus. The nucleus will enter an excited state and then emit secondary radiation to become stable. The release of this secondary radiation is used for the detection and measurement of thermal neutrons. The absorption cross section for many nuclei has been found to vary inversely with its velocity (5). When the velocity of a neutron is decreased through moderation the absorption cross section increases.

2.3 Photoneutron Production

When photons of high enough energy strike a nucleus, the nucleus will enter an excited state at which point it will release a neutron. In order for the neutron to be produced, the absorbed photon must have energy greater than the binding energy of the neutron to the nucleus (6). Photoneutrons can also be produced by an electron interacting with the nucleus; however, the direct portion of neutrons produced by electrons is at least two orders of magnitude smaller than neutron production by photons and is typically considered negligible. (6).

Photoneutron production is dependent on the photoneutron cross section of the material in which the photon interacts. A larger photoneutron cross section means there is greater probability of interaction occurring. Photoneutrons are produced in the giant dipole resonance region, primarily between 3 and 25 MeV, when the incident photon energy is above the production threshold energy (7). These threshold energies, (S_n), are listed in Table 1 for a few nuclides. Threshold energies typically range from 10 to 19 MeV for light nuclei ($A < 40$) and from 4 to 6 MeV for heavy nuclei (6).

Table 1: Reaction separation energies (8)

Element	Mass Number (A)	$S_n(\gamma,n)$ MeV
H	2	2.23
C	12	18.72
	13	4.95
Fe	54	13.38
	56	11.19
	57	7.65
	58	10.04
Ni	58	12.20
	60	11.34
	61	7.82
	62	10.60
	64	9.66
Cu	63	10.85
	65	9.91
W	180	8.41
	182	8.06
	183	6.19
	184	7.41
	186	7.20
Au	197	8.06
Pb	204	8.40
	206	8.09
	207	6.74
	208	7.37

Figure 6 is an example of a typical plot showing photonuclear cross sections for lead. The peak in the center is known as the giant resonance. This giant resonance curve varies from element to element with the midpoint given by the general formula $E_0 = 80A^{-1/3}$, where E_0 is in MeV and A is atomic weight (9). Using this equation the midpoint for lead is calculated to be approximately 13.5 MeV. In the energy region

of the giant dipole resonance the (γ, n) cross section for high Z elements is a factor of ten higher than for low Z elements (10).

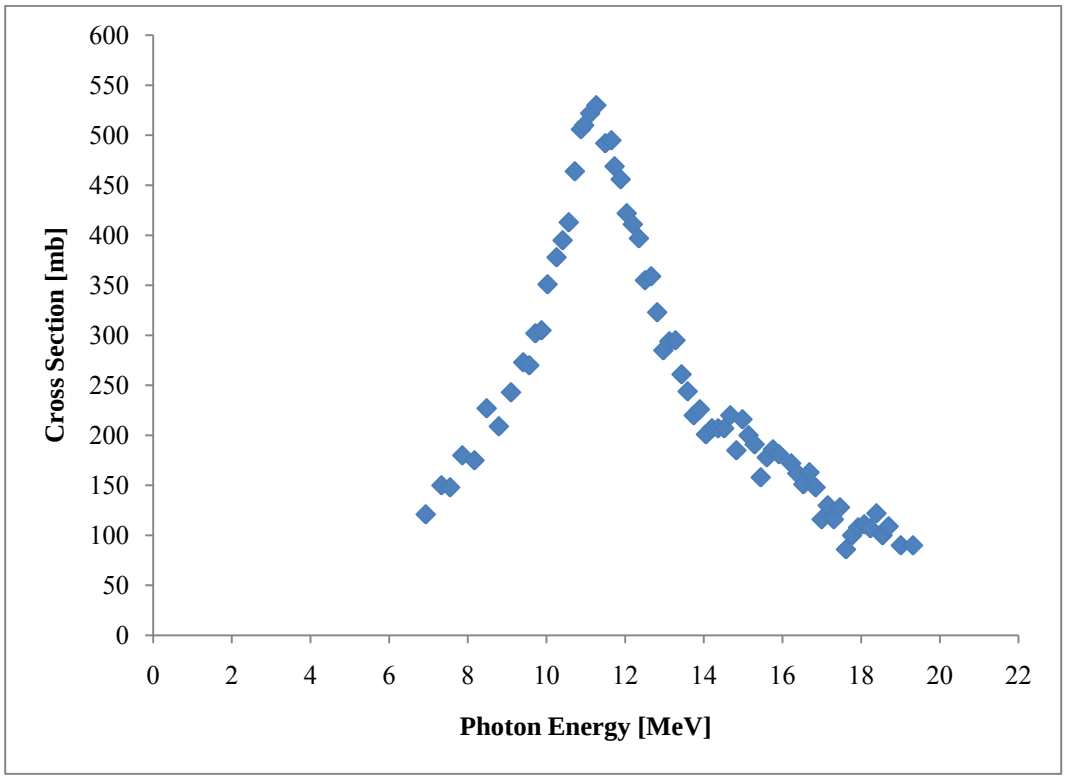

Figure 6: Photonuclear cross sections for lead (Graph reproduced from data measured by Harvey, *et al.)*

2.4 Photoneutrons in Radiation Therapy

In the United Sates, prostate cancer is the most common type of solid tumor in men, accounting for about 33% of new cancer cases and 10% of the cancer related deaths (12). There are a number of treatments used for treating prostate cancer, though the number of patients being treated with external beam radiation therapy has increased in recent years (13). Many of these patients are treated with higher energies

in order to achieve greater doses at deeper depths and to decrease skin dose. However, photons with energies greater than about 8 MeV can generate neutrons through photonuclear interactions with the accelerator's treatment head, patient's body, and treatment room (12). Some feel that the production of these neutrons is substantial enough to cause adverse side effects, unwanted dose and also induce secondary malignancies to the patient (14). Whereas others believe that the neutron dose is low enough to be neglected and consider treating with higher energy photons acceptable, assuming the benefits of treating with higher energies outweigh the risk associated with the added dose due to photoneutron production.

Linear accelerators are capable of producing neutrons through a photonuclear reaction. If the energy of the incident photon is high enough it can interact with the nucleus of an atom and excite the atom, causing the release of a neutron. These neutrons can be produced in the accelerator head, typically the collimators, target and flattening filter, and even the patient's body. The photoneutrons are produced isotropically and penetrate the head shielding in all directions (15). As the neutrons penetrate the shielding, a considerable degrading of the neutron spectrum follows (16). The average energies of the primary neutrons do not vary greatly with peak photon energies, as can be seen from Table 2 (16).

Table 2: Average neutron energies produced in linear accelerators (16)

Photon Energy [MV]	Average Neutron Energy [MeV]
15	1.8
20	2.1
25	2.2
30	2.4

It has been reported that photoneutron production is higher for dynamic fields, like those delivered during intensity modulated radiation therapy (IMRT), than static fields. IMRT refers to a radiation therapy technique in which a non-uniform fluence is delivered to the patient from any given position of the treatment beam to optimize the composite dose distribution (2). This treatment technique involves the use of a multileaf collimator which typically consists of 20-60 pairs of tungsten leaves that can each move independently. These leaves are 5 mm to 10 mm in width and offer the ability to attenuate or modulate the beam throughout the treatment.

The increased precision and conformity from modulating the intensity of the beam allows for the delivery of higher doses of radiation to the tumor site while sparing the normal tissue sounding the treatment area. However, when compared with more conventional radiotherapy techniques, the amount of beam on time for IMRT is typically longer because of the continuous moving of the MLC and modulation of the beam. Typically the number of monitor units used in IMRT is about 2 to 4 times higher than the total monitor units in conventional treatments (17). This increased amount of beam time and monitor units can result in more scatter dose and also more neutron production. It was once even reported that IMRT increases the risk of

secondary cancers from 1.00% for 6 MV x-rays to 24.4% for 25 MV x-rays when compared to conventional therapy (18).

2.5 Characteristics of High and Low Energy Photon Beams

Most conventional medical linear accelerators operate in the range from 6 MV to 25 MV. Depending on the location of the target, higher energy beams may improve treatment efficiency and result in an overall better treatment plan for the patient. The percentage depth dose is one way of characterizing a photon beam. The percentage depth dose (PDD) is defined as the percentage of absorbed dose at any depth relative to a fixed depth (2). The reference depth is usually taken to be the point of maximum dose. Higher energy beams have a greater penetrating power and thus a greater depth dose (2). This can be confirmed by the results of percentage depth dose data measured for the 6 MV and 23 MV beams of Linac C as seen in Figure 7.

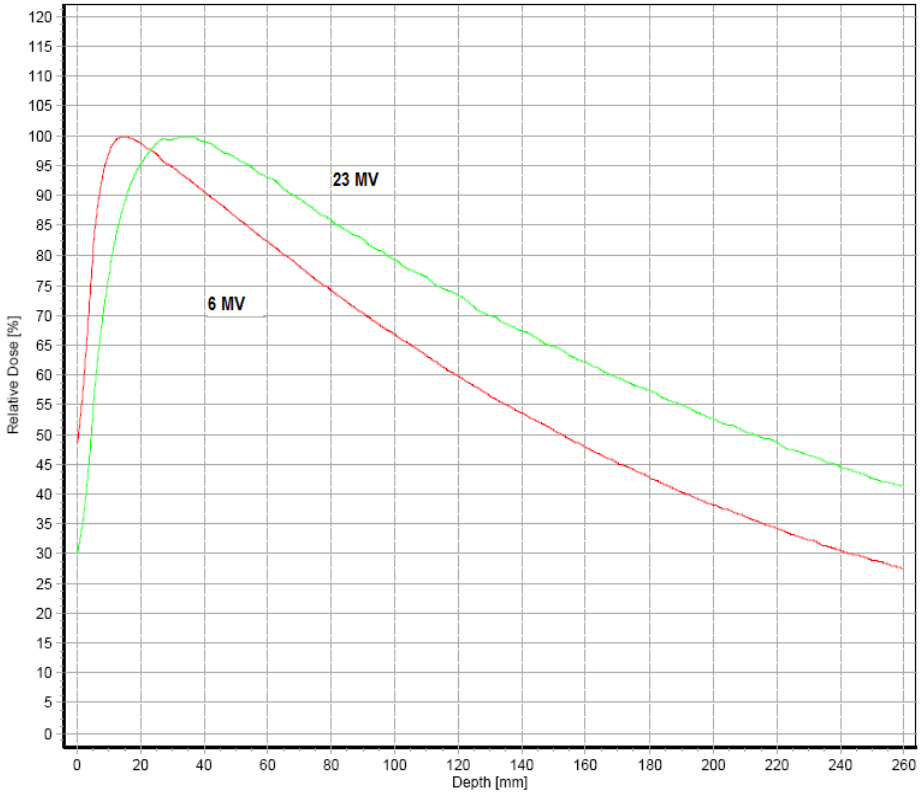

Figure 7: 6 MV and 23 MV percentage depth dose for Linac C

From the graph in Figure 7, one can see the higher energy beam has a lower entrance dose and a deeper d_{max} value. D_{max} for the 6 MV of this linac is 1.5 cm and 3.5 cm for the 23 MV beam. The lower energy beam produces the maximum ionization closer to the skin surface, which is not necessarily desirable when treating lesions at greater depths. The higher energy beam allows for skin sparing, which is one of the most desirable features of high-energy photons beams (2). Due to the skin sparing effect and the ability to drive dose to greater depths, high energy photon beams are very often used clinically. Therefore, many patients potentially may be exposed to the neutrons generated by the high energy photons and their interactions

within the treatment head. For that reason it is important to have accurate knowledge of the neutron field associated with the photon beam.

2.6 Neutron Detection

Neutrons are indirectly ionizing, so neutron detection is based on measuring the secondary events generated through the nuclear reactions. Practically all types of neutron detectors involve a combination of a target material designed to carry out this conversion together with a more conventional type detector (19). Neutron monitoring can be divided into two categories: active monitoring and passive monitoring. Each type of monitoring requires a different type of detector. Active monitoring involves the use of the fluence and rem meters and passive monitoring uses detectors such as activation foils, solid state track detectors and bubble detectors.

2.6.1 Fluence and Rem Meters

Thermal detectors are used for active neutron monitoring. For this technique the fast neutrons must first be moderated until the thermal energies can be detected by a thermal neutron detector. Many commercial rem-meters use polyethylene as the moderator surrounding the thermal neutron detector (20). Rem-meters have a response that is proportional to dose equivalent, making these detectors useful when the neutron spectrum is not known. The BF_3 detector is a gas filled detector that, when combined with a polyethylene moderator, offers a dose equivalent-like response for thermal to 10 MeV neutrons (20). Knowledge of the neutron spectrum is required for fluence meters. Fluence meters have the ability to monitor variations in the

neutron field over time which make this detector suitable for intensity modulated radiation therapy measurements (20).

2.6.2 Activation Detectors and Etched Track Detectors

Activation detectors use a material that when exposed to a neutron field becomes radioactive. The irradiated foil is then counted using a liquid scintillation counter. The measure of radioactivity correlates to the neutron fluence incident on the foil. Gold and indium foils are often used for thermal neutron detectors. A bare activation detector of phosphorous can be used to measure both thermal and fast neutron fluences (20).

Etched track detectors are based off the principle that heavy charged particles will leave radiation damage tracks in solids. This can occur when neutrons interact with the nuclei of the detector material and produce recoil nuclei, which leave damage trails (20). The irradiated sample will be etched and any radiation tracks present in the solid will be visible with the use of a microscope. These radiation tracks can provide insight into the characteristics of the neutron beam, including neutron dose equivalent.

2.6.3 Neutron Bubble Detectors

Bubble Technology Industries manufactures many of the neutron detectors used for medical linear accelerator monitoring. The neutron-detecting "bubble detector" has been used by government, military, scientific agencies and medical facilities for over 15 years and is a proven, patented technology (21). Bubble detectors have varied sensitivity, so they can be used to provide accurate data in

locations everywhere from the primary radiation field to the console area outside of the accelerator vault. Many neutron measurement devices lack the ability to provide accurate information because of the interference in the readings from the intense primary photon field; however, neutron bubble detectors are insensitive to the photons and electrons produced by the accelerator (21).

Bubble detectors consist of a gel or transparent polymer in which micro-droplets of Freon have been dispersed (22). These micro-droplets remain stable until exposed to neutrons. Secondary charged particles from the neutron field cause the micro-droplets to transition from a liquid to a gaseous state. The bubbles are formed instantly and can be easily read by the naked eye or counted with an automatic bubble reader. The number of bubbles formed will be directly related to the neutron dose equivalent. By varying the formulation of the detector liquid and the polymeric medium, the radiation detection properties of the bubble detector can be varied to meet different requirements (23).

The BD-PND (Bubble Detector Personal Neutron Dosimeter), as shown in Figures 8 and 9, is approximately 15 cm in length and 2 cm in diameter at the cap. The detector is activated by unscrewing the piston at the top. Once the cap is removed the detector will begin to measure neutron radiation and produce bubbles as seen in Figure 9. To reset the BD-PND, simply rethread the piston back to its original position. This will recompress all the bubbles after approximately 30 minutes, making the detector reusable.

Figure 8: BD-PND bubble dosimeters

Figure 9: Irradiated bubble dosimeter showing bubble formation

Bubble detectors can be used for many different applications. Such applications include neutron dosimetry, spectrometry, space and high altitude research, radon detection, medical linear accelerator monitoring and even soil sample "hot spot" analysis (23). An increasing area of use is that in the medical field for medical linear accelerator monitoring. The BD-PND is suitable for both measurements in and out of the primary radiation field making the detector ideal for

measuring photoneutron dose in the primary beam and also measuring neutron dose around the accelerator and vault for shielding calculations.

2.7 Neutron Shielding

In order for fast neutrons to be absorbed, they must first be slowed down through a series of interactions. A combination of materials for neutron shielding is typically used to achieve moderation. First, a material is needed that can moderate the neutrons through a series of elastic and inelastic scattering events. Once the neutron has reached thermal energies it can be captured by a nucleus. Hydrogen is extremely effective at removing energy from a beam of neutrons because of its low mass number. Each interaction with a hydrogen atom can reduce the neutron energy by approximately one-half. This makes water an excellent option for slowing down fast neutrons. Polyethylene has also been used in place of water because it contains 18% more hydrogen per unit volume than that of water (24).

Once the neutrons have been moderated, a material is needed that can capture the thermal neutrons. Using a material with a high neutron absorption cross section will increase the probability of absorption. Boron is often used in neutron shielding because of its higher absorption cross section. Boron can also be combined with polyethylene to absorb the thermal neutrons. Many of the shielding materials that are used to capture neutrons produce photons or gamma rays after absorption. A thin sheet of metal, such as lead or tungsten, can be used to shield the capture gamma rays and photons.

2.7.1 Vault Design

Radiotherapy machines must have sufficient shielding for scattered photons, and if the accelerator has the capability of producing higher energy photons, then extra shielding must be included to account for photoneutron production and interactions. Neutrons can induce radioactivity through neutron activation. Neutron capture can lead to the release of photons or gamma rays. Therefore, the proper selection and order of shielding material is crucial. Figure 10 provides a typical example of a treatment room floor plan for a medical linear accelerator showing the primary and secondary walls along with the maze and isocenter.

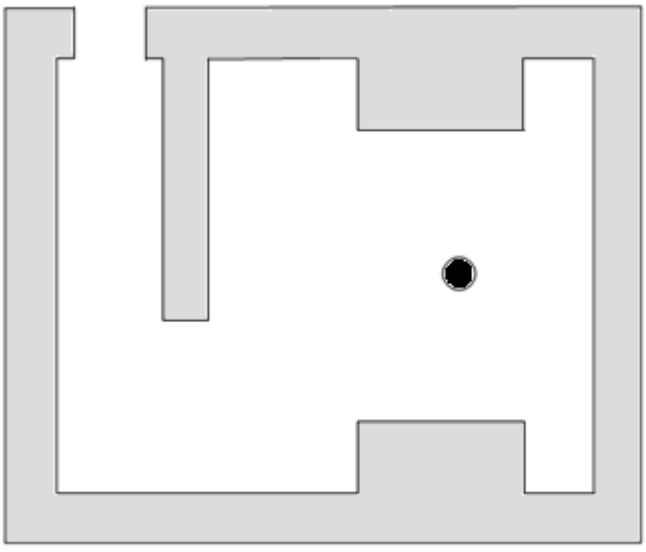

Figure 10: Basic linear accelerator treatment room floor plan showing primary and secondary walls, maze and isocenter

A variety of factors must be considered in the shielding design for a medical linear accelerator vault. These factors include: ALARA, available space, regulatory limits, shielding materials and therapy unit energy capabilities. The National Council on Radiation Protection and Measurements (NCRP) Report No. 151 provides technical information and recommendations regarding the structural shielding, design and evaluation of megavoltage x-ray and gamma-ray radiotherapy facilities.

2.7.2 Radiation Safety Survey

If the primary and secondary walls of vaults containing high energy linacs are made of concrete, then they are normally considered sufficient for shielding against photoneutrons generated through (γ, n) interactions. Concrete has a high hydrogen content which is very efficient at attenuating neutrons. The photoneutrons from medical linear accelerators have a tenth-value layer (TVL) of 21 cm in concrete, and the primary x-ray beam has a TVL of approximately 44 cm in concrete (15). This means that a concrete primary or secondary wall that attenuates the primary beam will be more than adequate for shielding the photoneutrons. The treatment door requires additional shielding for high energy machines to both properly moderate and capture the neutrons. In order to ensure that all radiation dose levels are below regulations, a radiation safety survey of the treatment vault and surrounding area must be performed prior to clinical operation.

There are several factors that must be considered when performing radiation safety surveys and calculations on medical linear accelerator vaults. According to NCRP Report No. 151 (20) consideration of the following factors should be made:

- Is the area considered a controlled or uncontrolled area?
- What is the workload for the radiotherapy machine?
- What is the use factor for a given barrier?
- How long are individuals occupying a specific area?
- Is the barrier a primary or secondary barrier?

Controlled areas are limited access areas in which the occupational exposure of personnel to radiation is under the supervision of an individual in charge of radiation protection (20). Access to these controlled areas is limited to personnel who are trained in the use of ionizing radiation and who have individually monitored exposure levels (20). A controlled area would be the console area outside of the vault where the therapists operate the accelerator, any workstations in the console area, and also the area near the vault door. Examples of uncontrolled areas would include patient exam rooms, restrooms, hallways and any area accessible by not only trained radiation staff, but also members of the general public.

The workload (W) for radiotherapy machines is the time integral of the absorbed dose rate determined at the depth of the maximum absorbed dose, 1 m from the source (20). The workload is estimated based on the approximate number of patients being treated each week and the number of monitor units or dose delivered to

each patient. For shielding calculations the units of W are expressed in Gy/week or MU/week.

The use factor (U) describes the amount of time that the primary beam is directed towards a barrier. Most modern day linear accelerators are capable of rotating 360 degrees around an isocenter. Therefore, a uniform distribution of gantry angles is assumed with the four primary angles being at 0, 90, 180 and 270 degrees (20). A use factor of 0.25 is typically appropriate for these types of accelerators.

The occupancy factor (T) is the factor by which the workload should be adjusted to correct for the degree or type of occupancy in a specific area (5). This factor accounts for the fraction of time that an individual is present in the area while the beam is on. Occupancy factors for controlled areas are considered to be one, whereas occupancy factors for uncontrolled areas are based on the amount of time that a single person spends in that location. Suggested values for occupancy factors from NCRP Report No 151 can be seen in Table 3.

Table 3: Occupancy Factors (20)

Location	Occupancy Factor (T)
Full occupancy areas (offices, treatment planning rooms, nursing stations, waiting rooms, etc.)	1
Adjacent treatment room or exam room	1/2
Corridors, lounges, staff restrooms	1/5
Vault Door	1/8
Public restrooms, storage rooms, unattended waiting rooms, attics	1/20
Outdoor areas with only pedestrian or vehicular traffic, unattended parking lots, stairways, unattended elevators	1/40

Radiation from a radiotherapy machine consists of both the primary beam and scattered radiation. A primary barrier will receive radiation directly from the source, whereas a secondary barrier will receive scattered radiation. Scattered radiation can potentially be emitted in all directions, while primary radiation is limited by the placement of the accelerator and maximum beam size (20). Primary barriers are sufficient enough to shield against any scattered radiation, but secondary barriers need to be designed to shield against leakage radiation, scattered radiation from patient and walls, and also secondary radiation such as photoneutrons.

2.7.3 Door Design

A maze in an accelerator room is used to help decrease radiation levels at the entrance of the vault by increasing the number of scattering events before the radiation is incident on the vault door. However, if floor space is minimal, a maze may be eliminated and a direct shielded door used in its place. Direct shielded doors help to

free up space and reduce the amount of walking required by the therapists, but there are some disadvantages associated with this. Direct shielded doors are very heavy and expensive, especially for vaults that contain high energy linacs (25).

Door shielding in high-energy rooms is usually dominated by the neutron capture gamma ray and photoneutron requirements (20). A thermal neutron will undergo capture reactions with a range of materials and, depending on the material, a gamma ray of significant energy may be released. The average energy of a capture gamma ray is 3.6 MeV, but the spectrum extends to beyond 8 MeV (15).

A vault door for a high energy linac typically consists of a steel case 0.635 cm thick containing 10.2 cm of borated polyethylene (5% boron) and a 1.27 cm lead slab (15). Boron is often incorporated into polyethylene because of its high neutron capture cross section for thermal neutrons and also because the capture gamma is of a lower energy, 0.478 MeV. A thin sheet of lead is placed after the borated polyethylene to shield against the capture gamma rays. The entire door is housed in a still casing that attenuates any low energy photons not shielded by the lead.

2.7.4 Treatment Head Leakage

Most of the materials located within the accelerator head are heavy elements which are good for photon shielding, but poor for neutron shielding. The generation of photoneutrons in the treatment head, as well as the scattering of photons, both contribute to the accelerator head leakage. Accelerator head leakage is dependent on the materials found in the treatment head and also the amount of time the radiation

beam is on. According to *Mutic, et al.,* facilities that treat with dynamic MLC must consider head leakage because of the increased number of monitor units and beam on time required of dynamic treatments (26). The radiation levels of photons and neutrons that are leaked through the head shielding are regulated by most states. These regulations as described by McGinley are outlined below (15).

1. The absorbed dose from neutrons and photons due to head leakage must not exceed 0.1% of the absorbed dose from x-rays at the isocenter for any point along a circular plane of 2 meters centered on and perpendicular to the central axis at isocenter (15).

2. Points outside the patient area and at 1 meter from the path of the electron beam shall not receive an absorbed dose to photons of greater than 0.1% of the x-ray dose at isocenter or 0.05% due to neutrons.

2.8 Neutron Dose

Neutron interactions in soft tissue can occur with oxygen, carbon and nitrogen, although the dominate interaction occurs primarily with hydrogen nuclei because it represents the largest number of atoms in tissue (27). The mass of a neutron is similar to that of hydrogen nuclei, resulting in a larger energy transfer per collision for fast neutrons. The first collision interaction is the largest contributor of dose in tissue because neutrons can deposit all of their energy in a single head-on collision with a hydrogen atom. Thermal neutrons transfer energy through absorption. The (n, γ)

interaction with hydrogen releases a capture photon of 2.225 MeV, which may also deposit some of its energy in the body (24).

Doses from different types of radiation are not all equivalent in terms of radiobiological effects. For example, there are higher rates of cataracts among physicists working in cyclotron laboratories whose eyes have been exposed over a long period of time to neutron radiation (5). This is due to the fact that neutrons have been found to be much more efficient at producing cataracts than gamma radiation (5).

In order to account for the different biological effectiveness of the different types of radiation, a system of radiation weighting factors has been adopted. A radiation weighting factor is a dimensionless number assigned to each type of radiation depending on its relative biological effectiveness (RBE). Radiation weighting factors range from 1, for x-ray and gamma-ray radiation, and up to 20 for alpha particles and neutrons. Table 4 provides a complete list of radiation weighting factors for each specific type of radiation. The dose equivalent, which is equal to the absorbed dose in Gray multiplied by the radiation weighting factor, is given in units of Sieverts.

Table 4: Radiation Weighting Factors (5)

Radiation	W_R
x-ray, gamma-ray, beta radiations (all energies)	1
Neutrons	
Thermal	5
0.01 MeV	10
0.1 MeV	10
0.5 MeV	20
> 0.1 - 2 MeV	20
> 2 - 20 MeV	10
> 20 MeV	5
High-energy protons	5
Alpha particles, fission fragments, heavy nuclei	20

3 MATERIALS AND METHODS

3.1 Detectors and Linear Accelerators

3.1.1 Neutron Bubble Detectors

Temperature compensated BD-PND Bubble Dosimeters were used for all neutron measurements. According to the calibration certificates provided by Bubble Technology Industries, all bubble detectors were calibrated to an Am-Be source at a distance and time that produced 100-150 bubbles. The detectors were calibrated 5 times at different temperatures between 20°C to 37°C and the average response was recorded as the calibration number. Table 5 presents the calibration data for each detector provided by Bubble Technology Industries. For all neutron measurements completed in this research the bubble detectors were read four times, each time rotating the detector one quarter of a turn.

Table 5: Bubble Dosimeters Calibration

Detector Number	Bubbles/mrem	Bubbles/uSv
10112228	32	3
10117135	30	2.8
10117148	33	3
10117215	31	2.9
10117224	30	2.8
10161138	1.2	0.11
10161150	0.98	0.092
10161155	0.91	0.085
10161201	1.1	0.1
10161248	0.76	0.071

The difference in mrem to uSv is not a constant value of 10 due to the differences in the NCRP (National Council on Radiation Protection) and ICRU (International Commission on Radiation Units and Measurements) recommendations for neutron dose equivalents for Americium – Beryllium sources. According to NCRP Report 38, the recommended neutron dose equivalent for a neutron fluence of 1 neutron per square centimeter is 3.84×10^{-5} mrem. ICRU Report 66 recommends a neutron dose equivalent for the same fluence of 4.11×10^{-4} uSv. The ratio of these two numbers provides a neutron dose equivalent of 10.7 uSv/mrem for AmBe.

3.1.2 Linear Accelerators

Three Varian linear accelerators were used for data collection for the measurements included in this report. The energies for each accelerator are listed in Table 6. The linear accelerators will be referred to as Linac C, H, or L.

Table 6: Linear accelerators

Linear Accelerator	Energy [MV]	Representation
Varian Trilogy	6, 23	Linac C
Varian Trilogy	6, 10	Linac H
Varian 23 EX	6, 15	Linac L

3.2 Dose Correction Factors

3.2.1 Monitor Unit Linearity Correction

The naked eye was used for counting the bubbles in the bubble detector. In order to accurately count the bubbles it was desired that fewer than 50 bubbles be produced in each detector for each measurement. For many of the measurements this required that the linear accelerator only be running for a few seconds. This short amount of time would produce enough bubbles for accurate counting.

For each measurement the linac would be set to deliver a certain number of monitor units. Linear accelerators are calibrated to deliver 1 cGy of absorbed dose per monitor unit (MU) at a depth of dmax at 100 cm SAD (source-axis-distance) or at 100 cm SSD (source-surface-distance) in water. Monitor units can be delivered in increments of 1 MU. It is important to know that the dose delivered per MU is linear even down to a few monitor units. To verify that the dose per MU is in fact linear, a monitor unit linearity test was performed on the Varian Trilogy Linac C.

Using an ionization chamber and electrometer, monitor unit linearity measurements were taken for the 23 MV beam. The chamber was positioned at the

end of the table with the chamber hanging off the edge. The buildup cap was left in place. The center of the chamber was at 100 cm SCD (source-chamber-distance) and the chamber was centered longitudinally and laterally using the cross hair and room lasers. A 10 x 10 cm^2 field size was set by the collimators. A series of measurements were taken for a range of monitor unit settings, from 2 MU to 600 MU. The average output for 100 MU was calculated for each MU setting. An average of all outputs was used to calculate the deviation of each monitor unit setting output from the overall average. If the deviation from the mean was considered significant, a correction factor could be applied to neutron measurements that were taken for small monitor unit settings. This correction factor would help to ensure the validity of the neutron measurements.

3.2.2 Application of the Inverse Square Law

It was desired that some of the results from the neutron measurements be reported in units of mSv of neutron dose per cGy of absorbed photon at isocenter (mSv/cGy). The Varian Trilogy Linac C was calibrated to deliver 1 cGy/MU at 100 SSD + dmax. As a result, any measurements not performed at this geometry would require corrections for the inverse square.

The inverse square law states that the intensity of the radiation decreases proportionally to the square of the distance from the source. For the Varian Trilogy Linac C some measurements were made at 100 cm SAD, but the accelerator was calibrated to deliver 1 cGy/ MU at 103.5 cm. The ratio of the two numbers squared

would provide the correction needed to calculate absorbed dose at 100 cm SAD. From the calculation Linac C will deliver 1.071 cGy/MU at 100 SAD (96.5 SSD, 3.5 cm depth). The photon doses at isocenter for the 3 linear accelerators used in this report are listed in Table 7 below.

$$\frac{I_1}{I_2} = \left(\frac{r_2}{r_1}\right)^2 \qquad \textbf{(Equation 3)}$$

$$I_2 = 1\frac{cGy}{MU} * \left(\frac{103.5}{100}\right)^2 = 1.071\ cGy/MU$$

Table 7: Isocenter dose [cGy/MU]

Linear Accelerator	Energy [MV]	Calibration	cGy/MU at Isocenter
Linac C	6	100 SSD + dmax (101.5 cm)	1.030
Linac H	10	isocenter	1.000
Linac L	15	100 SSD + dmax (103 cm)	1.061
Linac C	23	100 SSD + dmax (103.5 cm)	1.071

3.3 Field Size Dependency

Neutron field size dependence measurements were performed in air at isocenter (100 cm SCD). The bubble dosimeters were positioned at the end of the treatment table, aligning the cross hair and lasers to the center of the collecting volume, as shown in Figure 11. Two to five monitor units were given for each measurement to ensure that the detectors were not over dosed and still readable by the naked eye. The field sizes considered were 5 x 5 cm^2, 10 x 10 cm^2, 20 x 20 cm^2 and 40 x 40 cm^2.

Figure 11: Bubble detector hanging off edge of treatment table at 100 SCD

3.4 Off-Axis Measurements

Neutron measurements were performed at isocenter and at varying distances along the patient plane. These off axis measurements were completed at 5, 10, 20, and 50 cm off-axis. Measurements were completed both in air and water for field sizes ranging from 5 x 5 cm^2 to 40 x 40 cm^2. Figure 12 is a representation of measurements taken in air for the 23 MV photon beam.

Figure 12: Off-axis measurements in air

3.5 Neutron Dose as a Function of Depth in Water

A small water phantom and a Wellhofer water phantom were used to investigate the variation of neutron dose equivalent with increasing depth in water for the Linac H and Linac C as shown in Figure 13. These measurements were completed at 100 cm SSD for field sizes ranging from 5 x 5 cm^2 to 40 x 40 cm^2. All measurements were completed on the central axis. Measurements were taken at depths ranging from 1 cm to 25 cm in water.

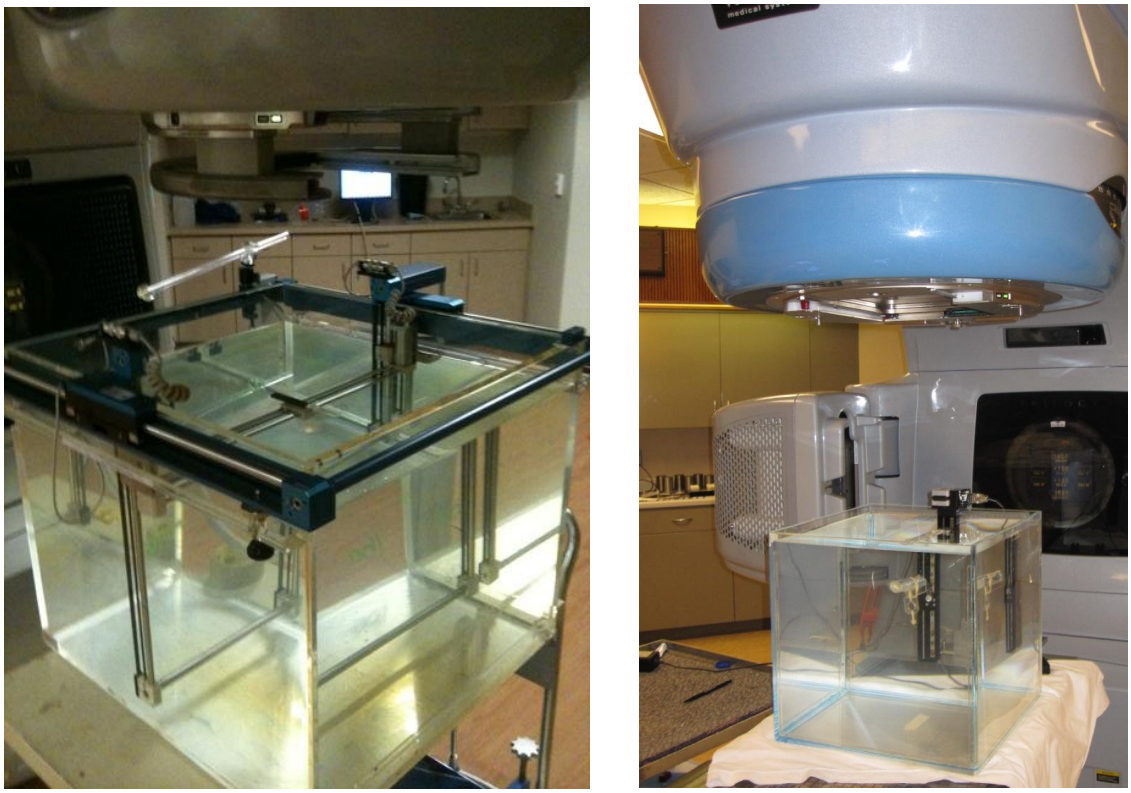

Figure 13: Neutron depth dose measurements with chamber centered on central axis at a 10 cm depth

3.6 IMRT Photoneutron Production

Three 23 MV IMRT prostate plans were measured on Linac C using the neutron bubble detectors. Measurements were taken in water at 90 SSD at a 10 cm depth. Measurements were taken 15 cm superior to isocenter. This setup would mimic the setup of IMRT prostate patients and provide a neutron dose equivalent that these patients would receive to the abdomen.

Each IMRT plan delivered 180 cGy per fraction for 43 fractions for a total dose of 7740 cGy. The bubble detectors were used to measure a single fraction for each plan. Without appropriate shielding, the detector would produce too many bubbles to be read by the naked eye. Borated polyethylene (BPE) was used to decrease the intensity of the neutrons to a point that would allow for accurate and readable measurements.

The bubble detectors were placed in a water phantom at a 10 cm depth and then surrounded by 5 cm of borated polyethylene as shown in Figures 14 and 15. The chambers were positioned laterally in the radiation field to reduce the dose gradient across the chamber from the IMRT plan. A shielding factor for the 5 cm of BPE was measured using the same geometry (90 SSD, 10 cm depth) as used for the IMRT measurements. A 10 x 10 cm^2 field size was irradiated alone in water and then again with the BPE shielding the detector in the water. The ratio of these two readings would provide the factor for which the neutron dose equivalent would be reduced as a result of using the BPE.

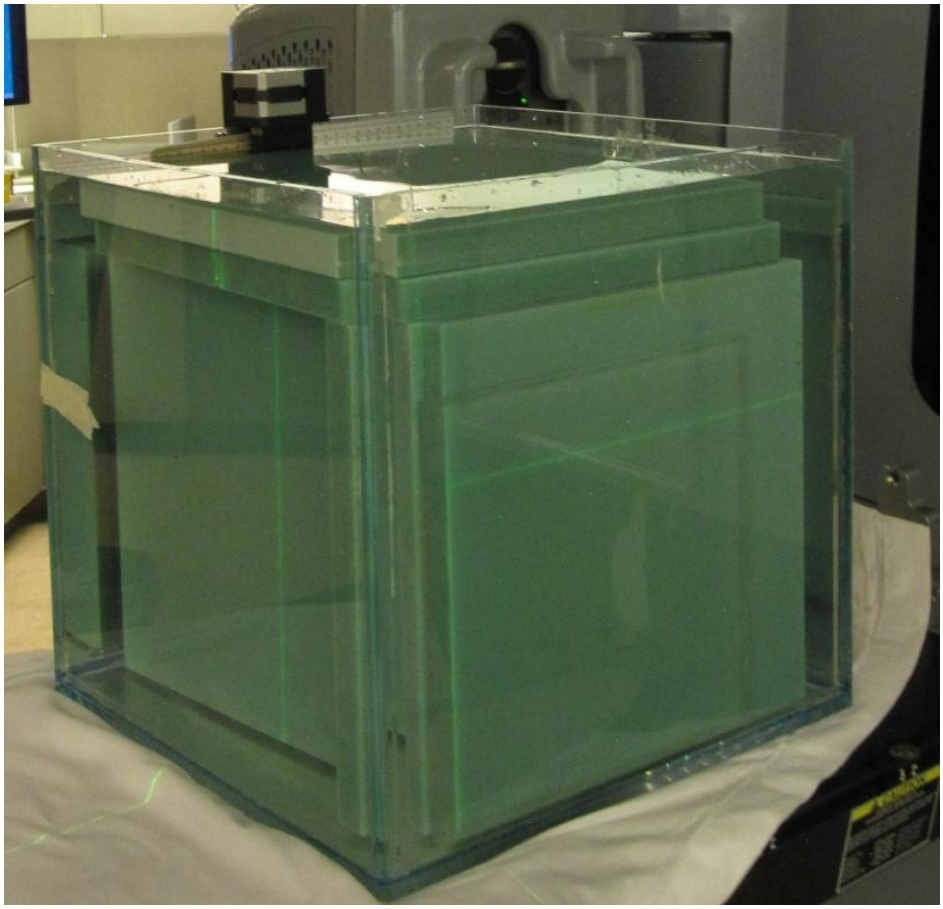

Figure 14: IMRT water phantom with 5 cm of BPE surrounding bubble detector

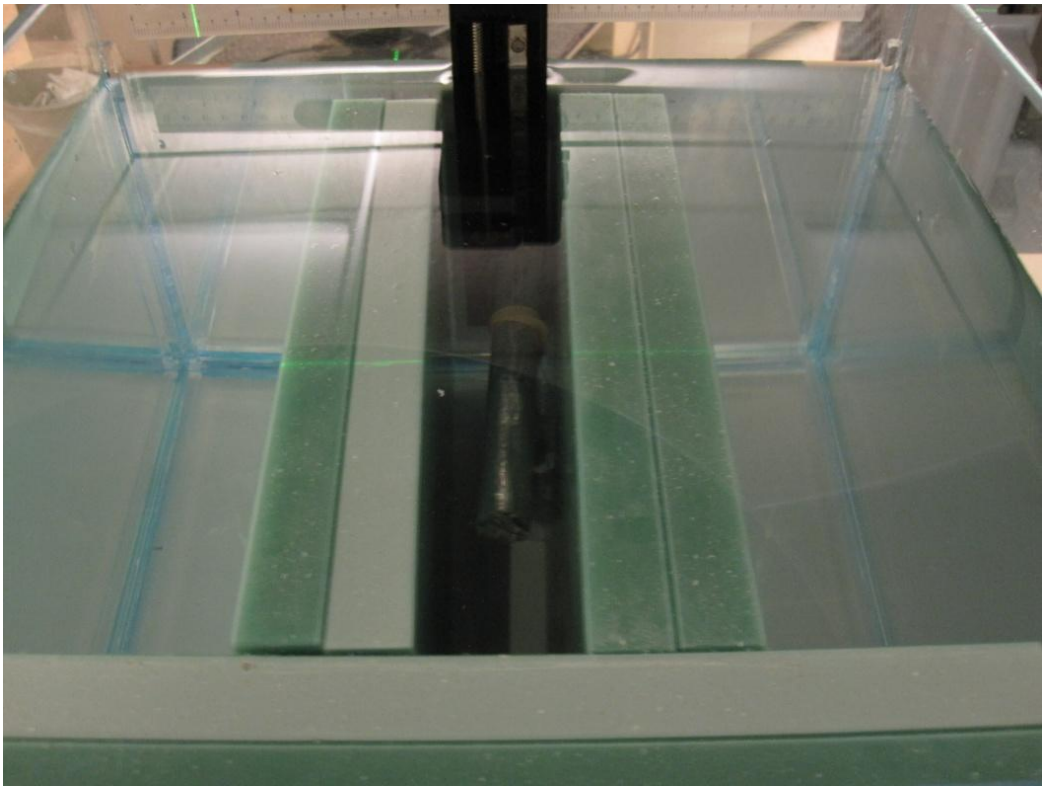

Figure 15: Inside view of IMRT water phantom with detector located at a 10 cm depth

4 RESULTS

4.1 Monitor Unit Linearity Analysis

The output for the Trilogy Linac C was measured for a MU setting of 2 MU to 600 MU. The linear relationship between machine output and monitor units can be seen in Figure 16. The graph is almost perfectly linear until approximately the 5 MU setting. A maximum standard deviation of 2.5% was observed for the 2 monitor unit setting. Above a monitor unit setting of 5 MU only a fraction of a percent was seen for all standard deviations. To ensure accuracy of measurements taken for 2 MU, a 2.5% correction factor was applied to the raw data. Any differences in linearity for monitor unit settings above 2 MU would be considered negligible.

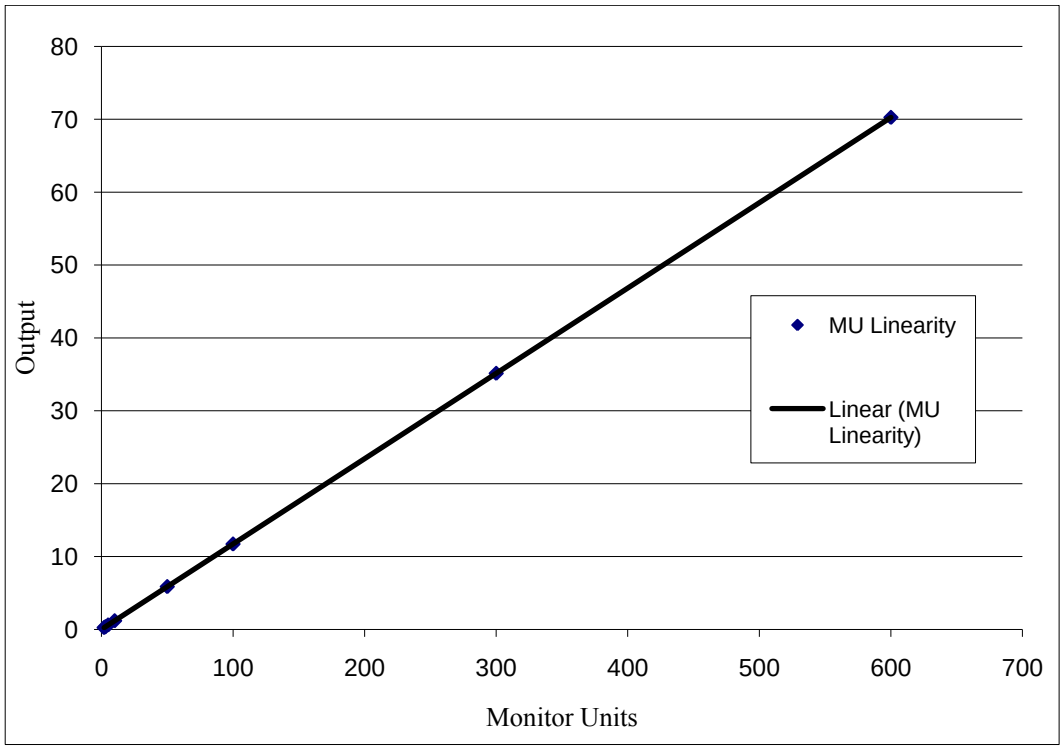

Figure 16: Monitor units vs. Linac C output

4.2 Neutron Dose Field Size Dependency

The variation of neutron dose with field size was analyzed for the 15 MV beam of Linac L and the 23 MV beam of Linac C. Measurements were completed using bubble dosimeters at 100 cm SAD in air. The results of these measurements are listed below in Table 8. The maximum neutron dose equivalent was measured for the 20 x 20 cm^2 field for both the 15 and 23 MV beams. The smallest neutron dose equivalent was measured for the 5 x 5 cm^2 field for both the 15 and 23 MV beam.

Table 8: Field size dependency 15 MV (top) and 23 MV (bottom)

Linac L - 15 MV	
Field Size [cm]	**uSv/MU**
5	27
10	57
20	71
40	70

Linac C - 23 MV	
Field Size [cm]	**uSv/MU**
5	112
10	135
15	140
20	152
40	146

4.3 Off-Axis Neutron Dose Equivalent

The off-axis neutron dose equivalent was measured for Linac C, Linac L and Linac H. These off-axis measurements provide a good representation of the entrance neutron dose equivalent in the patient plane. Measurements were made both in air and water for the 15 MV beam and only in air for the 10 and 23 MV beam. Table 9 below gives the resulting data for the 10 MV beam. Data was taken in air for a 10 x 10 cm^2 field. The maximum neutron dose equivalent for the 10 MV was found to be 7 uSv/MU at isocenter.

Table 9: Linac H - 10 MV off-axis neutron dose equivalents in air

Linac H - 10 MV	
10 cm x 10 cm	
Detector Position [cm]	uSv/MU
0	7
5	3
10	2
15	1
20	1
50	1

The measurements listed in Tables 10 & 11 for the 15 MV and 23 MV beams were measured in air with the chamber centered at 100 SSD. Data were collected for 4 field sizes starting at isocenter and ending at 50 cm from the central axis. The maximum neutron dose equivalent was located at isocenter for all field sizes. From 20 to 50 cm off-axis the neutron dose equivalent did not vary greatly for any of the

fields. The 20 x 20 cm^2 had the highest neutron dose equivalent of 71 uSv/MU at isocenter for 15 MV and 194 uSv/MU for 23 MV.

Table 10: Linac L- 15 MV off-axis neutron dose equivalents in air

Linac L - 15 MV	
5 cm x 5 cm	
Detector Position [cm]	**uSv/MU**
0	41
5	27
10	23
20	18
50	16

Linac L - 15 MV	
10 cm x 10 cm	
Detector Position [cm]	**uSv/MU**
0	57
5	50
10	33
20	14
50	16

Linac L - 15 MV	
20 cm x 20 cm	
Detector Position [cm]	**uSv/MU**
0	71
5	56
10	42
20	33
50	18

Linac L - 15 MV	
40 cm x 40 cm	
Detector Position [cm]	**uSv/MU**
0	70
5	54
10	45
20	15
50	14

Table 11: Linac C- 23 MV off-axis neutron dose equivalents in air

Linac C - 23 MV	
5 cm x 5 cm	
Detector Position [cm]	uSv/MU
0	106
5	63
10	58
20	27
50	31

Linac C - 23 MV	
10 cm x 10 cm	
Detector Position [cm]	uSv/MU
0	168
5	129
10	46
20	33
50	34

Linac C - 23 MV	
20 cm x 20 cm	
Detector Position [cm]	uSv/MU
0	194
5	168
10	151
20	49
50	32

Linac C - 23 MV	
40 cm x 40 cm	
Detector Position [cm]	uSv/MU
0	190
5	189
10	178
20	82
50	31

Measurements for the 15 MV beam of Linac L were completed at 100 SSD at a 3 cm depth in water. The results of these measurements are listed in Table 12. The maximum neutron dose was measured for the 40 x 40 cm^2 field at isocenter. The neutron dose equivalent at 15 and 20 cm off-axis is almost constant for all field sizes.

Table 12: Linac L - 15 MV off-axis neutron dose equivalents in water

5 cm x 5 cm	
Detector Position [cm]	**uSv/MU**
0	27
5	22
10	19
15	15
20	16

10 cm x 10 cm	
Detector Position [cm]	**uSv/MU**
0	39
5	25
10	18
15	14
20	19

20 cm x 20 cm	
Detector Position [cm]	**uSv/MU**
0	49
5	34
10	31
15	18
20	19

40 cm x 40 cm	
Detector Position [cm]	**uSv/MU**
0	54
5	36
10	33
15	22
20	20

4.4 Neutron Dose Equivalent as a Function of Increasing Depth in Water

4.4.1 15 MV Photon Beam

The neutron dose equivalent as a function of depth in water was measured for the 15 MV photon beam of Linac L. Measurements were taken at a depth of 1, 5, 10, 15 and 25 cm in water. The results of these measurements can be seen in Tables 13 and 14. The highest neutron dose equivalent, 68 uSv/MU, was measured at a depth in water of 1 cm for the 40 x 40 cm^2 field. The lowest neutron dose equivalent, 35 uSv/MU, was measured for the 5 x 5 cm^2 field at a depth of 1 cm. For all field sizes

the neutron dose changed little from a depth of 15 cm to a depth of 25 cm. The average neutron dose equivalent at 25 cm in water for all field sizes was found to be 11±1 uSv/MU.

Table 13: 15 MV 5 cm x 5 cm (left) and 10 cm x 10 cm (right) neutron dose equivalent as a function of increasing depth in water

5 cm x 5 cm	
Detector Depth [cm]	**uSv/MU**
1	35
5	27
10	17
15	15
25	11

10 cm x 10 cm	
Detector Depth [cm]	**uSv/MU**
1	48
5	31
10	20
15	12
25	12

Table 14: 15 MV 20 cm x 20 cm (left) and 40 cm x 40 cm (right) neutron dose equivalent as a function of increasing depth in water

20 cm x 20 cm	
Detector Depth [cm]	**uSv/MU**
1	65
5	38
10	31
15	14
25	12

40 cm x 40 cm	
Detector Depth [cm]	**uSv/MU**
1	68
5	45
10	24
15	17
25	10

4.4.2 23 MV Photon Beam

The results of the neutron dose equivalent measurements a function of depth in water for the 23 MV beam can be seen in Table 15. Measurements were made for a 10 x 10 cm^2 field. The highest neutron dose equivalent was measured at a depth of 3 cm with the smallest dose equivalent measured at 22 cm.

Table 15: Neutron dose equivalent per monitor unit as a function of depth in water

10 cm x 10 cm	
Detector Depth [cm]	**uSv/MU**
3	162
4	122
5	82
10	64
15	54
20	40
22	31

4.5 Off-axis IMRT measurements

4.5.1 Determination of shielding attenuation factor for 5 cm of borated polyethylene

The results of the shielding measurements using BPE can be seen in Table 16. The neutron dose equivalent was found to be 0.97±0.05 uSv/MU for the BPE shielded detector. The unshielded detector (Table 17) had a neutron dose equivalent of 4.13±0.09 uSv/MU. The ratio of shielded to unshielded measurements was found to be 0.24. All off-axis IMRT measurements using this shielding thickness would be corrected by this factor.

Table 16: Neutron dose equivalent 15 cm off-axis at a 10 cm depth in water for a 10x10 cm^2 field with detector shielded by 5 cm of BPE

Trial	SSD [cm]	depth [cm]	MU	Detector No.	Bubbles/ uSv	Bubbles avg	bubbles/ MU	uSv/ MU
1	90	10	50	10161155	0.085	4	0.08	0.94
2	90	10	150	10161150	0.092	14	0.10	1.03
3	90	10	150	10161248	0.071	10	0.07	0.94

Table 17: Neutron dose equivalent 15 cm off-axis at a 10 cm depth in water for a 10x10 cm^2 field

Trial	SSD [cm]	depth [cm]	MU	Detector No.	Bubbles/ uSv	Bubbles avg	bubbles/ MU	uSv/ MU
1	90	10	40	10161248	0.071	12	0.30	4.23
2	90	10	40	10161201	0.1	17	0.41	4.13
3	90	10	40	10161155	0.085	14	0.34	4.04

4.5.2 Neutron dose equivalent for IMRT prostate plans

The neutron dose equivalents for the IMRT measurements taken with the shielded detector are listed in Table 18. The borated polyethylene reduced the neutron fluence enough to allow for accurate counting of the detectors. The neutron dose equivalent for the 180 cGy photon dose was found to be 377±26 uSv, or 2.1±0.1 uSv/cGy. The data listed in Table 18 does not yet have the neutron attenuation correction factor applied.

Table 18: IMRT off-axis measurements taken with 5 cm BPE surrounding detector

Plan	SSD [cm]	depth [cm]	Dose to Isocenter [cGy]	Detector No.	Bubbles/uSv	Bubbles avg	uSv	uSv/cGy
1	90	10	180	10161248	0.071	28	387	2.2
2	90	10	180	10161201	0.100	35	348	1.9
3	90	10	180	10161150	0.092	37	397	2.2

The attenuation factor for the 5 cm of BPE was applied to data in Table 19. This factor was determined through measurement to be 0.24. Meaning there was a 76% reduction in neutron fluence across the detector when using the BPE for shielding. The corrected neutron dose equivalent from the data average in Table 19 gives an average neutron dose equivalent of 8.92±0.62 uSv/cGy.

Table 19: Corrected IMRT off-axis neutron dose equivalent

Plan	Neutron Dose Equivalent w/ BPE [uSv/cGy]	Shielding Correction Factor	Corrected Neutron Dose Equivalent [uSv/cGy]
1	2.15	0.24	9.16
2	1.93	0.24	8.21
3	2.20	0.24	9.38

At 15 cm off axis the average neutron dose equivalent for the three IMRT plans, each delivering a total photon dose of 7740 cGy, was found to range from approximately 63 mSv to 73 mSv with the average being 69.02±4.78 mSv. Table 20 provides the results for the individual plans.

Table 20: IMRT Neutron Dose Equivalent 15 cm Off-Axis

Plan	SSD [cm]	depth [cm]	Isocenter Dose [cGy]	Fractions	Total Photon Dose [cGy]	Corrected Neutron Dose Equivalent [uSv/cGy]	Neutron Dose Equivalent [mSv]
1	90	10	180	43	7740	9.16	70.87
2	90	10	180	43	7740	8.21	63.58
3	90	10	180	43	7740	9.38	72.59

5 DISCUSSION

5.1 Neutron Dose Equivalent as a Function of Collimator Setting

The graph in Figure 17 provides a visual representation of the change in neutron dose as a function of increasing field size for the 15 MV and 23 MV beams. Although the neutron dose is significantly higher for the 23 MV beam, both graphs exhibit similar characteristics. The maximum neutron dose for both beams was measured for a 20 x 20 cm^2 field with a minimum change in neutron dose from a 20 x 20 cm^2 field to a 40 x 40 cm^2 field. This seems to suggest that a 20 x 20 cm^2 field produces the maximum neutron dose equivalent, with no added neutron dose contribution from increasing the collimator setting beyond the 20 x 20 cm^2 field size. The neutron dose increased by a factor of 1.3 from a 5 x 5 cm^2 field to a 40 x 40 cm^2 field for the 23 MV beam and by 2.6 for the same collimator settings for the 15 MV beam. These results reveal an increased dependence on collimator setting for the lower energy photons.

According to Nath *et al.,* the average energy of a neutron produced from a 15 MV beam is 1.8 MeV, whereas a 25 MV beam produces neutrons with an average energy of 2.2 MeV (16). The lower energy neutrons generated in the target and flattening filters may be attenuated more by the tungsten collimators when compared to higher energy neutrons, thus resulting in more attenuation for smaller collimator settings. However, this reduction in neutron fluence would not be too significant considering the low capture cross section for tungsten, except for neutrons at thermal

energies. In fact, tungsten shielded machines only reduce the neutron fluence by approximately 15% (20). Therefore, the increased dependence on collimator setting for the lower energy photons must be related to the differences in the neutron spectrums and neutron scattering in the treatment head.

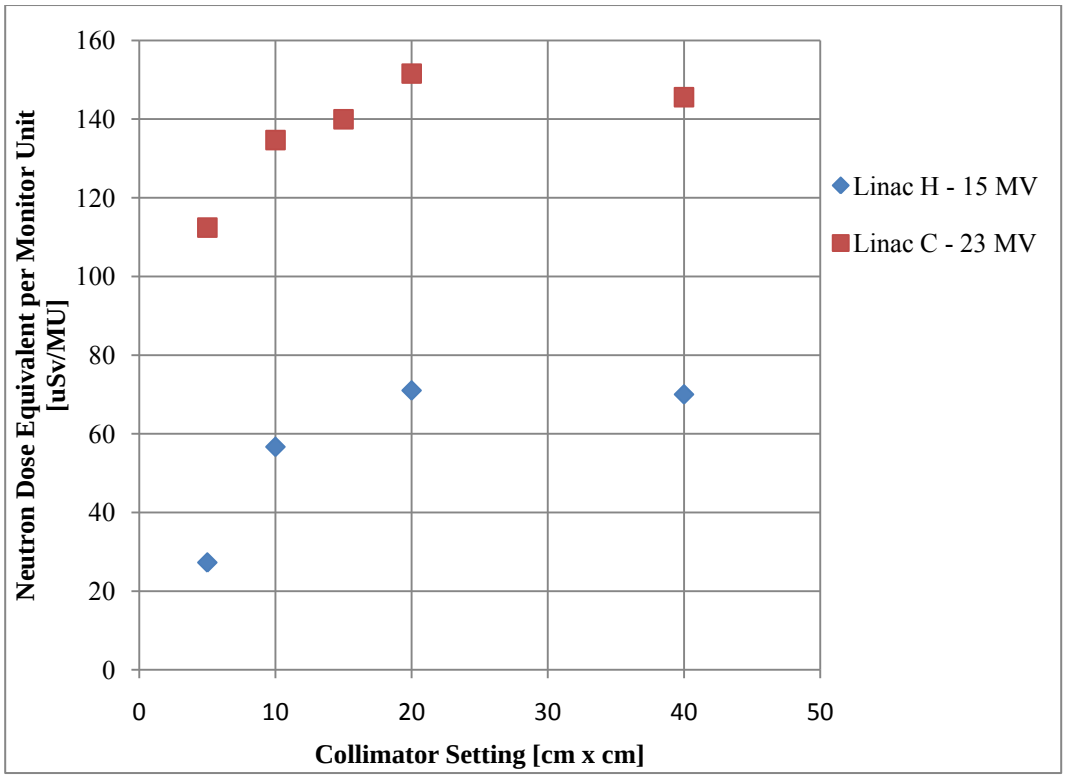

Figure 17: 15 MV and 23 MV neutron dose equivalent per monitor unit as a function of increasing field size

5.2 Variations in Neutron Dose Equivalent along Patient Plane

5.2.1 Entrance Neutron Dose Equivalent for a 15 MV and 23 MV Beam

The variation in neutron dose for the 15 MV and 23 MV photon beams from isocenter to 50 cm off-axis along the patient plane can be seen in Figures 18 and 19. The neutron dose equivalent was virtually the same at a distance of 50 cm from isocenter for all field sizes. According to d'Errico *et al.*, the reduction in neutron dose off-axis is due to the degrading of neutrons as they pass through the collimation system and shielding of the treatment head (28).

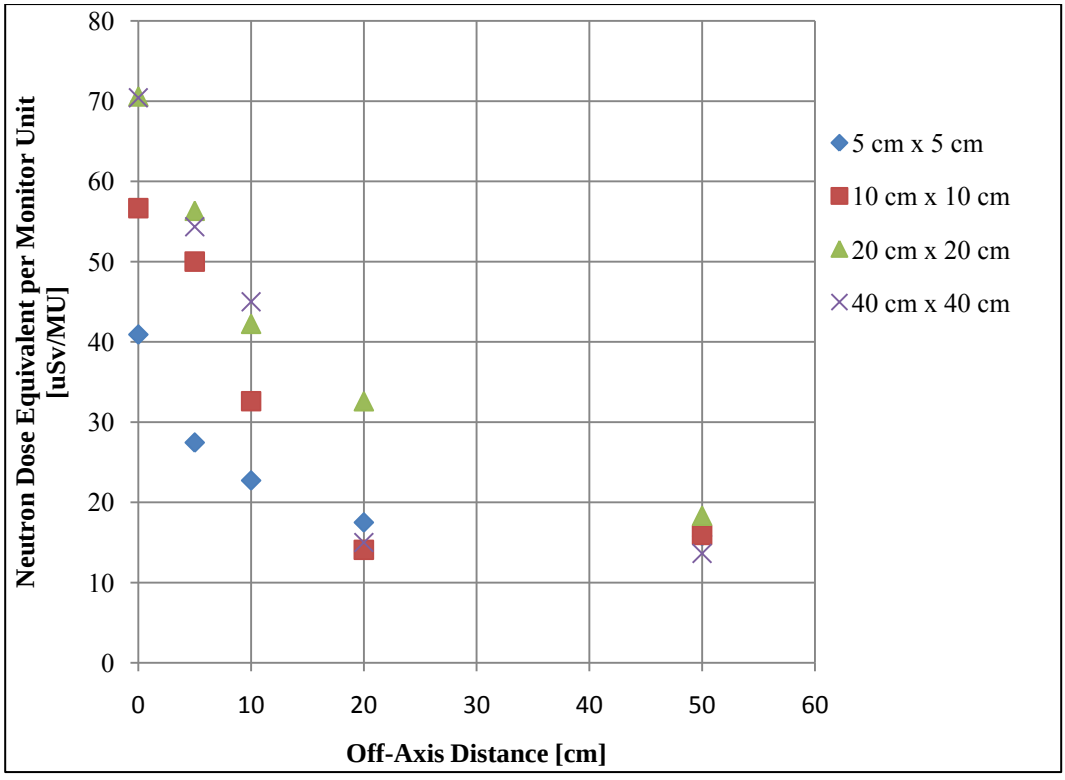

Figure 18: 15 MV off-axis neutron dose

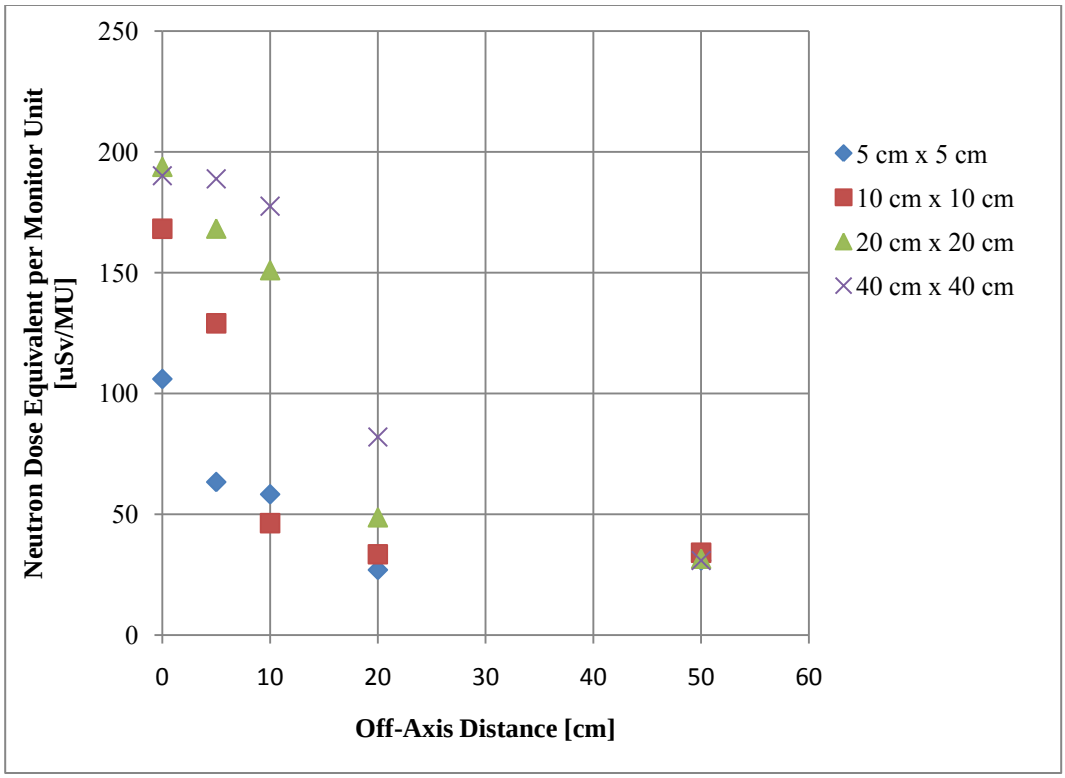

Figure 19: 23 MV off-axis neutron dose

The neutron dose equivalent per unit photon dose at isocenter was calculated for a 10 x 10 cm^2 field for the 10 MV, 15 MV and 23 MV beams as shown in Figure 20. The largest neutron dose equivalent of 15.7 mSv/Gy was calculated for the 23 MV beam at isocenter. This neutron dose is 2.8 times higher than that of the 15 MV beam and 24 times higher than the calculated neutron dose of the 10 MV beams. The low neutron dose for the 10 MV beam is evidence of the low photoneutron production that occurs for photon energies less than 10 MV.

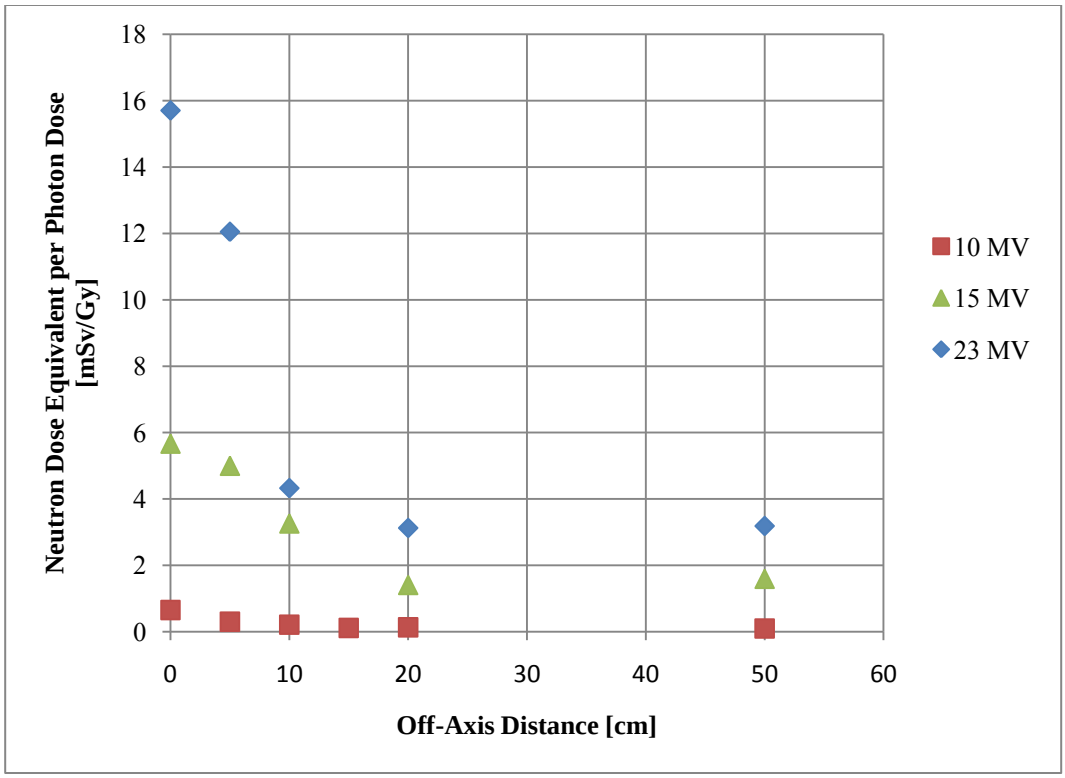

Figure 20: Neutron dose equivalent per photon dose as a function of increasing distance from isocenter

5.2.2 Off- Axis Neutron Dose Equivalent per Unit Photon Dose at a 3 cm Depth in Water for the 15 MV Beam

The neutron dose equivalent was measured at 100 SSD at a 3 cm depth in water along the patient plane for the 15 MV photon beam. These data, represented in Figure 21, are expressed in terms of neutron dose equivalent per absorbed photon dose at isocenter. The absorbed photon dose at isocenter for Linac L is 1 cGy/MU at 100 SSD and 3 cm depth for a 10 x 10 cm^2 field size. The maximum dose was measured at isocenter for the 40 x 40 cm^2 and was found to be 4.96 mSv/Gy. The dose off-axis at 20 cm for all field sizes is 1.81±.07 mSv/Gy.

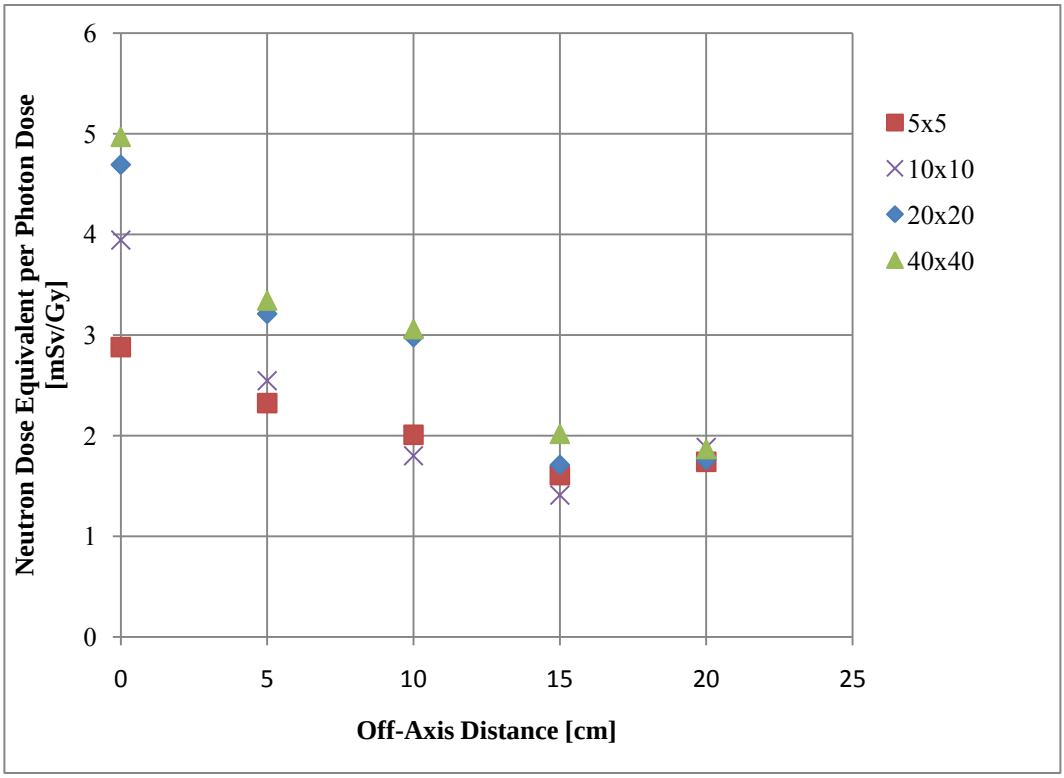

Figure 21: 15 MV neutron dose equivalent per unit photon dose, 3 cm deep in water along patient plane

The data in Figure 21 can be compared to measurements taken by others with similar geometries. These comparisons are listed in Table 21. Awotwi-Pratt *et al* (29) measured a dose of 1.4 mSv/Gy at a 1 cm depth and d'Errico *et al* (28) measured 4.5 mSv/Gy at a 1 cm depth. These are both lower than the 4.8 mSv/Gy that was measured for Linac L. The slight difference in energy and the different neutron detectors contribute highly to the variations in measured neutron dose.

Table 21: Measured neutron dose equivalent comparisons

Neutron dose equivalent per unit photon dose [mSv/Gy]					
Depth [cm]	**On Axis**	**10 cm off-axis**	**20 cm off-axis**	**Photon Energy [MV]**	**Reference**
1	4.5	2.1	1.8	18	d'Errico *et al*
1	1.4	-	-	15	Awotwi-Pratt *et al*
1	4.8	-	-	15	Present Work
3	4.7	1.8	1.9	15	Present Work
5	2.5	0.8	0.6	18	d'Errico *et al*
5	3.9	-	-	-	Present Work

5.3 Variation of Neutron Dose with Depth in Water for a 15 and 23 MV Photon Beam

5.3.1 Linac L – 15 MV

Figure 22 shows the variation of the neutron dose equivalent per monitor unit with depth in water for the 5 x 5 cm^2, 10 x 10 cm^2, 20 x 20 cm^2 and 40 x 40 cm^2 field sizes. A large variation in neutron dose for each field size is evident at the 1 cm depth. As the depth of water increases the neutron dose begins to vary less with field size. At 15 cm the average neutron dose equivalent is 15±2 uSv/MU. From 15 cm to 25 cm the neutron dose is approximately the same for all field sizes.

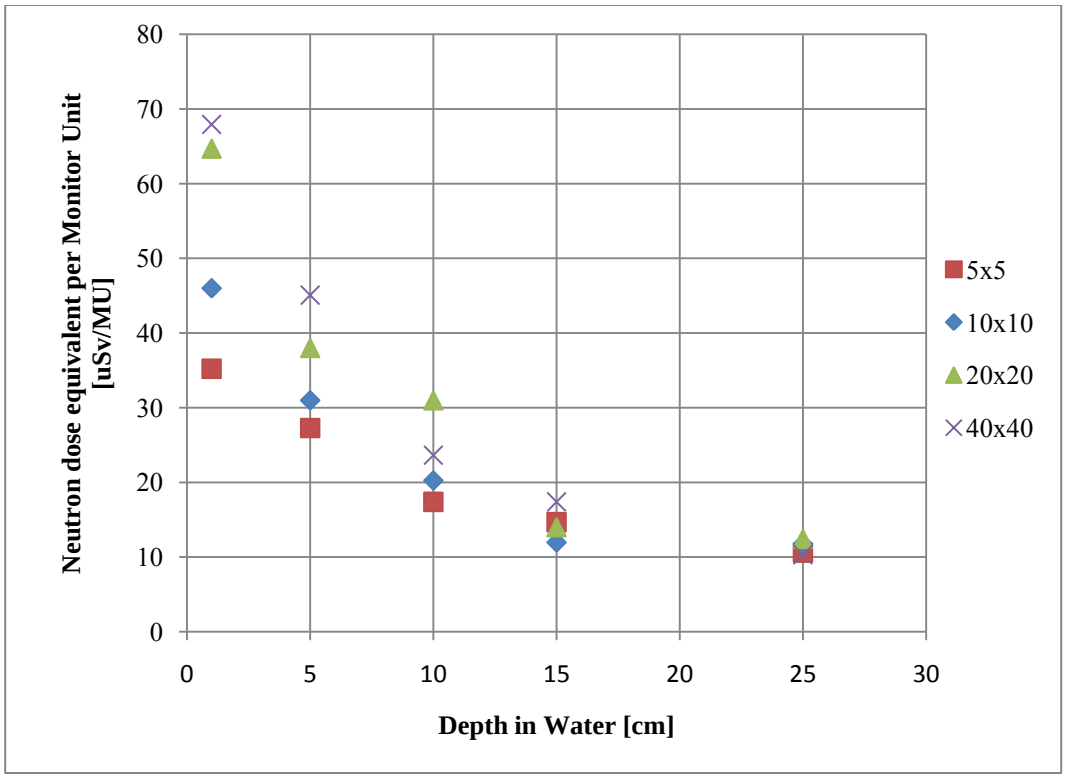

Figure 22: 15 MV Neutron dose equivalent in water

The photoneutrons emitted from the treatment head have a range of energies. The lower energy neutrons reach thermal equilibrium and are captured at shallower depths, while the higher energy neutrons travel longer distances before being captured. It is believed that the most energetic neutrons are found closest to the central axis since the most energetic photons that produce the neutrons in the forward direction are on the beam axis (29). This would explain the independence of neutron dose equivalent for field sizes at depths greater than 15 cm. At a greater depth the low energy neutrons have been captured; therefore, the neutron component is highest around the central axis and any increase in field size will not contribute to any added

neutron dose. Similar measurements were completed by *Awotwi-Pratt et al.,* who also measured an almost constant neutron dose equivalent independent of field size at greater depths (29).

5.3.2 Linac L – 23 MV

Neutron dose equivalent in water for the 23 MV linac revealed a sharp fall off in dose from a 3 cm depth to a 5 cm depth and then only a smaller decrease in dose past 5 cm as represented by Figure 23. The neutron dose begins to fall off because of the moderation and capture of the neutrons from the hydrogen nuclei.

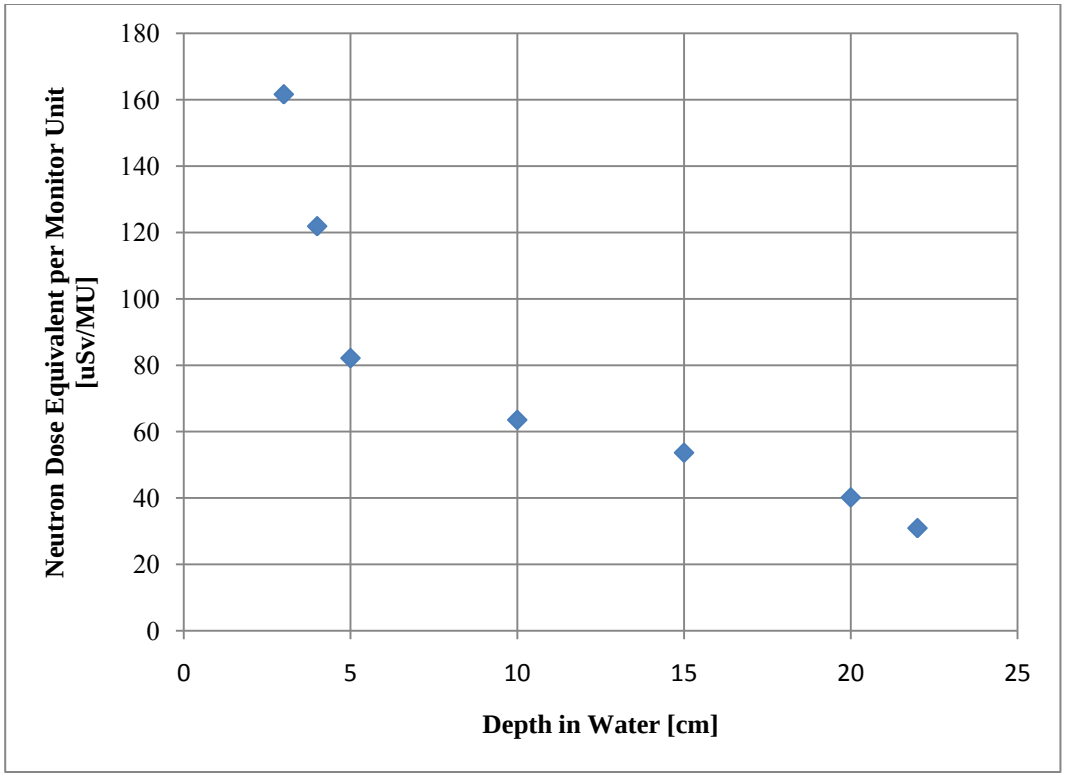

Figure 23: 23 MV Neutron dose equivalent in water

The photon dose for a 10 x 10 cm^2 field was determined using measured percentage depth dose (PDD) for the Linac C. The data is listed in Table 22. Photon doses per monitor unit were calculated at each depth. A radiation weighting factor of 1 for photons was used to convert the absorbed dose in Gray to a dose equivalent in Sieverts. Using the measured neutron dose equivalent and calculated photon dose, an increase in total dose was determined. The maximum increase in dose was found to be 1.6% at a depth of 3 cm on the beam central axis.

Table 22: Increase in total dose at depth due to neutrons

Depth [cm]	PDD	Photon Dose [Gy/MU]	Neutron Dose Sv/MU	Total Dose (Sv/MU)	Increase in Dose due to Neutrons
3	0.997	9.97E-03	1.62E-04	1.01E-02	1.6%
4	0.994	9.94E-03	1.25E-04	1.01E-02	1.3%
5	0.969	9.69E-03	8.42E-05	9.77E-03	0.9%
10	0.800	8.00E-03	6.51E-05	8.07E-03	0.8%
15	0.648	6.48E-03	5.50E-05	6.54E-03	0.8%
20	0.531	5.31E-03	4.12E-05	5.35E-03	0.8%
22	0.487	4.87E-03	3.17E-05	4.90E-03	0.7%

At a 3 cm depth it is evident that the higher energy neutrons have not achieved thermal equilibrium because of the 1.6% increase in dose equivalent at this point. However, as the depth increases more low energy neutrons are captured resulting in a decreased neutron dose. According to d'Errico *et al.,* the fast neutrons located within the primary beam contribute significantly to the total dose equivalent and their relative contribution increases with depth because of the attenuation of the low energy neutron fluence at a shallow depth (28).

5.4 Neutron Dose to Prostate Patients from Intensity Modulated Radiation Therapy

One concern for treating prostate patients with the higher energy beams is the neutron doses received in the abdominal region. Significant doses to this area could possibly add unnecessary dose to more radiosensitive organs and potentially result in secondary malignancies. Measuring the neutron dose off-axis for an IMRT plan would provide a good representation of neutron dose levels in this region.

According to McGinley, most medical accelerators that operate above 15 MeV produce neutron dose levels in the patient plane of approximately 1 to 2 mSv per Gy of x-ray dose at isocenter (15). The 1-2 mSv/Gy prediction by McGinley agrees well with the data measured for the IMRT plans. The IMRT plans averaged 0.9±0.1 mSv/Gy of absorbed x-ray dose at isocenter.

5.5 Neutron Dose Equivalent for IMRT versus Conventional Radiation Therapy

The neutron dose from 3 IMRT plans were compared with the neutron dose associated with conventional radiation therapy plans. The delivered dose was the same for both conventional and IMRT plans; however, the number of monitor units needed to deliver the dose changed substantially. The number of monitor units needed for the IMRT plans were nearly 3 times higher than the number of monitor units needed for the conventional plan as seen in Table 23.

Table 23: Monitor units required for IMRT vs. conventional treatment plan

Plan	IMRT MU	Conventional MU
1	702	216
2	590	210
3	657	220

The neutron dose equivalent associated with the 3 IMRT plans and 3 conventional plans are listed in Tables 24 and 25, respectively. From the data it can be seen that the neutron dose equivalent increased by approximately of factor of 1.8 for the plans delivered using IMRT. Similar measurements were made by Ipe *et al*., who noted a neutron dose increase by about a factor of 2 for IMRT treatments (17). This increase in neutron dose can largely be attributed to the increase in beam on time required of IMRT treatments. Although the number of monitor units needed for IMRT is approximately 3 times higher than what is needed for the conventional delivery, the neutron dose equivalent did not increase by the same factor of 3 as suggested by Howell, *et al.* (12). Ipe *et al*., did however measure similar increases in neutron dose for IMRT treatments. His results revealed an increase in neutron dose equivalent by a factor of 2, for an increase in monitor units of 3.8 (17).

Table 24: IMRT neutron dose equivalent per fraction

Plan	IMRT [uSv/Fraction]
1	1648
2	1479
3	1688

Table 25: Conventional plan neutron dose equivalent per fraction

Plan	Conventional [uSv/Fraction]
1	891
2	866
3	908

5.6 Neutron Dose Equivalent at Isocenter as a Function of Photon Energy

Figure 25 shows the variation of neutron dose equivalent as a function of photon energy. These measurements were taken for a 10 x 10 cm^2 field. The maximum neutron dose was measured for the 23 MV beam of Linac C and was found to be 14 mSv/Gy. The 15 MV beam of Linac L produced a neutron dose equivalent of 5 mSv/Gy. The 6 MV and 10 MV beams showed only a small amount of neutron dose. The threshold energy for photoneutron production varies for the different materials in the accelerator head, but most materials contained in the treatment head have threshold energies above 10 MV. This explains the almost negligible neutron production at this energy. Above 10 MV the photoneutron cross section increases for many of the materials resulting in an increased probability of photoneutron production which is evident by the results in Figure 24.

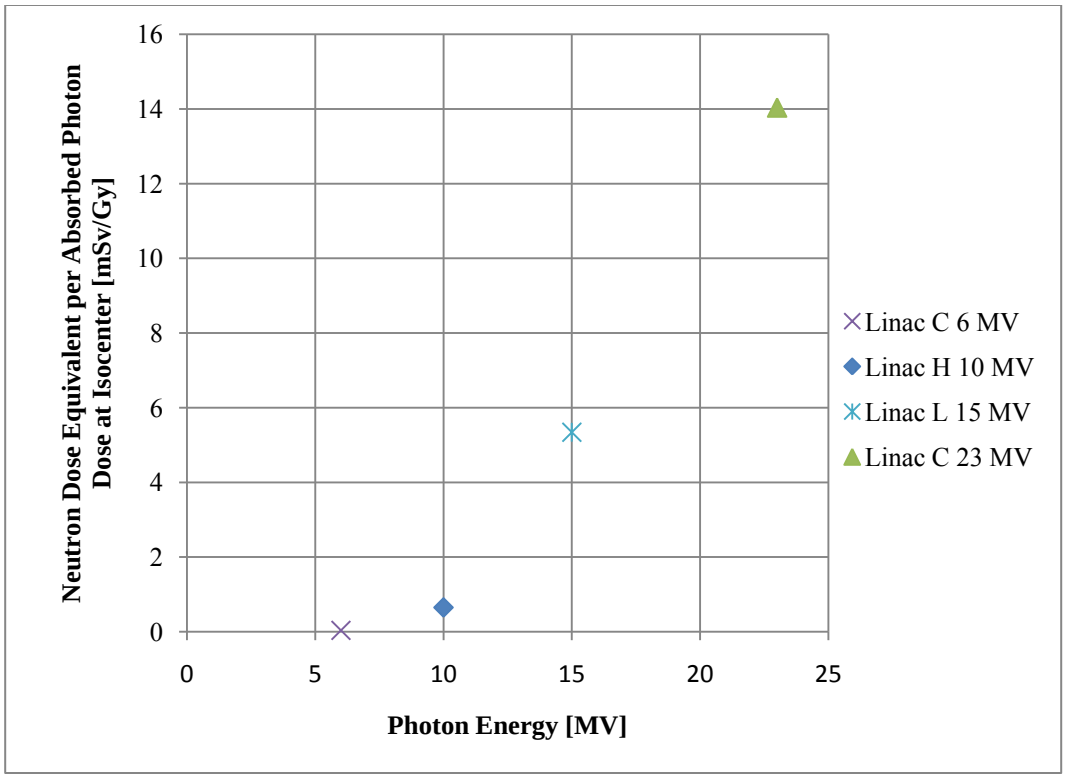

Figure 24: Neutron dose equivalent at the beam isocenter for per photon dose as a function of photon energy

6 CONCLUSION AND FUTURE WORK

6.1 Conclusion

The neutron dose received by patients from photoneutrons generated through (γ, n) interactions within medical linear accelerators was investigated for various field sizes, geometries and 3 IMRT prostate plans. Off axis neutron dose measurements revealed a neutron dose equivalent of 0.9±0.1 mSv/Gy for IMRT prostate plans. The neutron dose equivalent at isocenter was found to increase significantly from 0.64 mSv/Gy for a 10 MV beam to 14.04 mSv/Gy for a 23 MV beam. The off-axis neutron dose equivalent was also found to be approximately 2 times higher for IMRT when compared to conventional radiation therapy.

Based off the data measured in this report, the neutron field cannot be neglected. However, the benefits of treating with higher energy photons and IMRT may outweigh the risks associated with any secondary neutron dose and thus physicians may choose to ignore these risks to achieve an overall more effective treatment for the patient.

6.2 Future Work

Additional measurements could be taken in order to better understand the neutron production and associated patient dose. The measurements stated in this report could be investigated further in the following ways:

- Evaluate the responses of different types of neutron detectors in out and of the radiation field.

- Perform neutron measurements for IMRT plans from a 15 MV, 18 MV, and 23 MV beam.
- Choose appropriate detectors to determine the energy of the neutron field generated in the linear accelerator

BIBLIOGRAPHY

1. **Podgorsak, E.B.** *Radiation Oncology Physics: A Handbook for Teachers and Students.* Vienna : International Atomic Energy Agency, 2005.

2. **Khan, Faiz M.** *The Physics of Radiation Therapy.* Baltimore : Lippincott Williams & Wilkins, 2010.

3. **Shultis, J. Kenneth and Faw, Richard E.** *Radiation Shielding.* La Grange Park : Prentice Hall, 2000. 0-89448-456-7.

4. **Krane, Kenneth S.** *Introductory Nuclear Physics.* s.l. : John Wiley & Sons, 1988. 978-0-471-80553-3.

5. **Cember, Herman and Johnson, Thomas E.** *Introduction to Health Physics.* s.l. : The McGraw-Hill Companies, 2009. 978-0-07-142308-3.

6. *Neutron production from a mobile linear accelerator operating in electron mode for intraoperative radiation therapy.* **LoiG, Dominietto, M, et al.** Italy : Institute of Physics, 2006, Physics in Medicine and Biology, pp. 695-702.

7. *Monte Carlo study of photoneutron production in the Varian Clinac 2100C linac.* **Ma, A, et al.** 1, Budapest : Journal of Radioanalytical and Nuclear Chemistry, 2007, Vol. 276, pp. 119-123.

8. *Neutron contamination from medical electron accelerators.* Maryland : HP, 1984.

9. *High-energy Photons in IMRT: Uncertainties and Risks for Questionable Gain.* **Welsh, James S, Mackie, Thomas and Limmer, Jeffrey.** 2, s.l. : Adenine Press, 2007, Technology in Cancer Research and Treatment, Vol. 6. 1533-0346.

10. **Ongaro, Carla, et al.** *Analysis of photoneutron spectra produced in medical accelerators.* Torino : IPO Publishing Ltd, 2000.

11. **Harvey, RR, et al.** Photoneutron cross sections of Pb206, Pb207, Pb208. *Center for Photonuclear Experiments Data.* [Online] October 2010. http://cdfe.sinp.msu.ru/cgi-bin/search.cgi.

12. *Investigation of secondary neutron dose for 18 MV dynamic MLC IMRT delivery.* **Howell, Rebecca M, et al.** 3, Georgia : American Association of Physicists in Medicine, 2004, Vol. 32, pp. 786-793. 0094-2405.

13. *Primary radiation therapy for localized prostate cancer.* **Eng, TY, Thomas, CR and Herman, TS.** San Antonio : Semin Urol. Oncol., 2002, Vol. 7, pp. 239-257.

14. **Saeed, MK, et al.** *Doses to Patients from Photoneutrons emitted in a Medical Linear Accelerator.* s.l. : Oxford University Press, 2008.

15. **McGinley, Patton H.** *Shielding Techniques for Radiation Onocology Facilities.* Madison : Medical Physics Publishing, 2002. 1-930524-07-2.

16. **Nath, Ravinder, et al.** *Neutron Measurements Around High Energy X-Ray Radiotherapy Machines.* New York : American Insitute of Physics, 1986.

17. **Ipe, NE, et al.** *Neutron Measurements for Intensity Modulated Radiation Therapy.* Standford : s.n., 2000.

18. *Estimates of whole-body dose equivalent produced by beam intensity modulated conformal therapy.* **Followell, D, Geis, P and Boyer, A.** 38, Houston : s.n., June 1997, Int J Radiat Oncol Biol Phys , pp. 667-672.

19. **Knoll, Glenn F.** *Radiation Detection and Measurement.* s.l. : John Wiley & Sons Inc., 2000.

20. **National Council on Radiation Protection and Measurements.** *Structural Shielding Design and Evaulation for Megavoltage X- and Gamma- Ray Radiotherapy Facilities.* s.l. : National Council on Radiation Protection and Measurements, 2005.

21. Bubble Technology Industries: Bubble Detector. *Bubble Technology Industries.* [Online] 2004. [Cited: June 1, 2010.] http://www.bubbletech.ca/radiation_detectors_files/bubble_detectors.html.

22. **Bourgois, L, Delacroix, D and Ostrowsky, A.** *Use of Bubble Detectors to Measure Neutron Contamination of a Medical Accelerator Photon Beam.* s.l. : Nuclear Technology Publishing, 1997. pp. 239-246.

23. *Bubble Detectors - A Maturing Technology.* **Ing, H, Noulty, R A and McLean, T.D.** 1, Ontario : Elsevier Science Ltd. , 1997, Radiation Measurements, Vol. 27, pp. 1-11.

24. **Martin, James E.** *Physics for Radiation Protection.* New York : John Wiley & Sons, Inc., 2000.

25. **Biggs, Peter J.** *Radiation Shielding for Megavoltage Photon Therapy Machines.* Boston : s.n., 2010.

26. *Room shielding for intensity-modulated radiation therapy treatment facilities.* **Mutic, S, et al.** St. Louis : s.n., 2001, International Journal of Radiation Oncology Biology Physics, Vol. 50, pp. 239-246.

27. **Hall, Eric J. and Giaccia, Amato J.** *Radiobiology for the Radiologist.* Philadelphia : Lippincott Williams & Wilkins, 2006.

28. *In-phantom dosimetry and spectometry of photoneutrons from an 18 MV linear accelerator.* **d' Errico, Francesco, et al.** 9, September 1998, Medical Physics, Vol. 25, pp. 1717-1724.

29. *Measurement of photoneutrons in the output of 15MV Varian Clinac 2100C LINAC using bubble detecotrs.* **Awotwi-Pratt, JB and Spyrou, NM.** 271, Budapest : s.n., 2007, Journal of Radioanalytical and Nuclear Chemistry, Vol. 3.

30. *Handbook on Photonuclear Data for Applications: Cross-Sections and Spectra.* Austria : International Atomic Energy Agency, 2000. 1011-4289.

APPENDIX

Table 26: Monitor unit linearity for Linac C

MU	1	2	3	Mean	Rdg per 100 MU	% Diff From Mean
2	0.241	0.241	0.239	0.240	12.02	2.5
3	0.358	0.357	0.356	0.357	11.90	1.5
5	0.591	0.596	0.595	0.594	11.88	1.3
10	1.177	1.177	1.177	1.177	11.77	0.4
50	5.864	5.863	5.864	5.864	11.73	0.0
100	11.704	11.716	11.709	11.710	11.71	-0.1
300	35.130	35.130	35.130	35.130	11.71	-0.1
600	70.250	70.250	70.250	70.250	11.71	-0.1
Average Reading per 100 MU:					11.73	0.4

Table 27: Field size dependence for Linac C - Trial 1

Setup Parameters				Trial #	Distance [cm]		Collimator Setting	Temperature [°C]		
				1	100	SAD	As Indicated	26.7		
Notes:	In air measurements, detector hanging off end of table			Accelerator			Energy	Date		
				LINAC C			23 MV	9/21/2010		
Detector Number	Bubbles/ uSv	Field Size [cm]	MU	Bubble Count				Bubbles Average	Bubbles /MU	uSv/MU
				1	2	3	4			
1150	0.092	5	3	29	27	30	35	30	10	110
1248	0.071	10	5	47	52	44	44	47	9	132
1155	0.085	15	2	23	30	30	28	28	14	163
1138	0.11	20	2	32	32	30	30	31	16	141
1201	0.1	40	2	32	33	32	32	32	16	161

Table 28: Field size dependence for Linac C - Trial 2

Setup Parameters				Trial #	Distance [cm]		Collimator Setting	Temperature [°C]		
				2	100	SAD	As Indicated	26.7		
Notes:	In air measurements, detector hanging off end of table			Accelerator			Energy	Date		
				LINAC C			23 MV	9/21/2010		
Detector Number	Bubbles / uSv	Field Size [cm]	MU	Bubble Count				Bubbles Average	Bubbles /MU	uSv/MU
				1	2	3	4			
1150	0.092	5	2	22	22	19	24	22	11	118
1155	0.085	10	2	24	24	25	23	24	12	141
1138	0.11	15	2	27	27	27	28	27	14	124
1201	0.1	20	2	33	34	33	36	34	17	170
1248	0.071	40	2	20	19	20	19	20	10	137

Table 29: Field size dependence for Linac L

Setup Parameters				Trial #	Distance [cm]		Collimator Setting	Temperature [°C]		
				1	100	SAD	As Indicated	26.7		
Notes:	In air measurements, detector hanging off end of table			Accelerator			Energy	Date		
				LINAC L			15 MV	10//9		
Detector Number	Bubbles / uSv	Field Size [cm]	MU	Bubble Count				Bubbles Average	Bubbles/MU	uSv/MU
				1	2	3	4			
1138	0.11	5	3	9	9	9	9	9	3	27
1201	0.1	10	3	17	17	17	17	17	6	57
1155	0.085	20	3	18	18	18	18	18	6	71
1248	0.071	40	3	15	15	15	15	15	5	70

Table 30: Off-axis neutron dose equivalents for Linac H

Setup Parameters				Trial #	Distance [cm]		Collimator Setting	Temperature [°C]		
				1	100	SAD	10 x 10	26.7		
Notes:	In air measurements, detector hanging off end of table, isocentrically cal, 2.5cm dmax			Accelerator			Energy [MV]	Date		
				LINAC H			10	10/7/2010		
Detector Number	Bubbles / uSv	Detector Position [cm]	MU	Bubble Count				Bubbles Average	Bubbles /MU	uSv/ MU
				1	2	3	4			
1138	0.11	0	20	15	15	15	15	15	1	7
1201	0.1	5	50	15	15	15	15	15	0	3.
1248	0.071	10	100	15	15	15	15	15	0	2
1138	0.11	15	150	17	17	17	17	17	0	1
1201	0.1	20	150	20	20	20	20	20	0	1
1155	0.085	50	250	21	20	20	21	21	0	1

Table 31: Off-axis neutron dose equivalents for Linac L - 5 cm x 5 cm

Setup Parameters				Trial #	Distance [cm]		Collimator Setting	Temperature [°C]		
				2	100	SAD	5 cm x 5 cm	25		
Notes:	In air measurements, detector placed on treatment couch (only msd one side of iso to conserve sensitivity)			Accelerator			Energy	Date		
				Linac L			15 MV	10//9		
Detector Number	Bubbles/ uSv	Detector Position [cm]	MU	Bubble Count				Bubbles Average	Bubbles /MU	uSv/ MU
				1	2	3	4			
1138	0.11	0	2	9	9	9	9	9	5	41
1155	0.085	5	3	7	7	7	7	7	2	27
1138	0.11	10	4	10	10	10	10	10	3	23
1201	0.1	20	4	7	7	7	7	7	2	18
1155	0.085	50	8	11	11	10	11	11	1	16

Table 32: Off-axis neutron dose equivalents for Linac L - 10 cm x 10 cm

Setup Parameters				Trial #	Distance [cm]		Collimator Setting	Temperature [°C]		
				2	100	SAD	10 cm x 10 cm	25		
Notes:	In air measurements, detector placed on treatment couch (only msd one side of iso to conserve sensitivity)			Accelerator			Energy	Date		
				Linac L			15 MV	10//9		
Detector Number	Bubbles/ uSv	Detector Position [cm]	MU	Bubble Count				Bubbles Average	Bubbles /MU	uSv/ MU
				1	2	3	4			
10161201	0.1	0	3	17	17	17	17	17	6	57
10161201	0.1	5	2	10	10	10	10	10	5	50
10161150	0.092	10	3	9	9	9	9	9	3	33
10161248	0.071	20	4	4	4	4	4	4	1	14
10161201	0.1	50	8	13	12	13	13	13	2	16

Table 33: Off-axis neutron dose equivalents for Linac L - 20 cm x 20 cm

Setup Parameters				Trial #	Distance [cm]		Collimator Setting	Temperature [°C]		
				2	100	SAD	20 cm x 20 cm	25		
Notes:	In air measurements, detector placed on treatment couch (only msd one side of iso to conserve sensitivity)			Accelerator			Energy	Date		
				Linac L			15 MV	10//9		
Detector Number	Bubbles/ uSv	Detector Position [cm]	MU	Bubble Count				Bubbles Average	Bubbles /MU	uSv/ MU
				1	2	3	4			
1155	0.085	0	3	18	18	18	18	18	6	71
1248	0.071	5	2	8	8	8	8	8	4	56
1248	0.071	10	3	9	9	9	9	9	3	42
1150	0.092	20	4	12	12	12	12	12	3	33
1150	0.092	50	8	14	13	14	13	14	2	18

Table 34: Off-axis neutron dose equivalents for Linac L - 40 cm x 40 cm

Setup Parameters				Trial #	Distance [cm]		Collimator Setting	Temperature [°C]		
				2	100	SAD	40 cm x 40 cm	25		
Notes:	In air measurements, detector placed on treatment couch (only msd one side of iso to conserve sensitivity)			Accelerator			Energy	Date		
				Linac L			15 MV	10//9		
Detector Number	Bubbles/ uSv	Detector Position [cm]	MU	Bubble Count				Bubbles Average	Bubbles /MU	uSv/ MU
				1	2	3	4			
1248	0.071	0	3	15	15	15	15	15	5	70
1150	0.092	5	3	15	15	15	15	15	5	54
1201	0.1	10	4	18	18	18	18	18	5	45
1201	0.1	20	8	12	12	12	12	12	2	15
1138	0.11	50	8	12	12	12	12	12	2	14

Table 35: Off-axis neutron dose equivalents for Linac C - 5 cm x 5 cm

Setup Parameters				Trial #	Distance [cm]		Collimator Setting	Temperature [°C]		
				1	100	SAD	5 cm x 5 cm	25		
Notes:	In air measurements, detector placed on treatment couch (only msd one side of iso to conserve sensitivity)			Accelerator			Energy	Date		
				Linac C			23 MV	9/29/2010		
Detector Number	Bubbles /uSv	Detector Position [cm]	MU	Bubble Count				Bubbles Average	Bubbles /MU	uSv /MU
				1	2	3	4			
1201	0.1	0	2	23	21	21	22	22	11	109
1201	0.1	5	2	13	12	14	13	13	7	65
1150	0.092	10	2	11	10	11	12	11	6	60
1248	0.071	20	6	11	11	12	12	12	2	27
1155	0.085	50	4	7	7	8	20	11	3	31

Table 36: Off-axis neutron dose equivalents for Linac C - 10 cm x 10 cm

Setup Parameters				Trial #	Distance [cm]		Collimator Setting		Temperature [°C]	
				1	100	SAD	10 cm x 10 cm		26	
Notes:	In air measurements, detector placed on treatment couch			Accelerator			Energy		Date	
				Linac C			23 MV		9/23/2010	
Detector Number	Bubbles/ uSv	Detector Position [cm]	MU	Bubble Count				Bubbles Average	Bubbles /MU	uSv /MU
				1	2	3	4			
10161155	0.085	-50	4	15	17	16	15	16	4	46
10161138	0.11	-20	2	15	16	15	15	15	8	69
10161150	0.092	-10	2	12	12	12	12	12	6	65
10161248	0.071	-5	2	19	18	19	19	19	9	132
10161201	0.1	0	2	35	33	34	36	35	17	173
10161155	0.085	5	2	22	23	23	22	23	11	132
10161201	0.1	10	2	9	9	10	10	10	5	48
10161248	0.071	20	4	9	10	10	9	10	2	33
10161138	0.11	50	4	14	16	15	15	15	4	34

Table 37: Off-axis neutron dose equivalents for Linac C - 20 cm x 20 cm

Setup Parameters				Trial #	Distance [cm]		Collimator Setting		Temperature [°C]	
				1	100	SAD	20 cm x 20 cm		25	
Notes:	In air measurements, detector placed on treatment couch (only msd one side of iso to conserve sensitivity)			Accelerator			Energy		Date	
				Linac C			23 MV		9/29/2010	
Detector Number	Bubbles/ uSv	Detector Position [cm]	MU	Bubble Count				Bubbles Average	Bubbles /MU	uSv /MU
				1	2	3	4			
1201	0.1	0	2	40	40	39	40	40	20	199
1248	0.071	5	2	25	24	24	25	25	12	173
1150	0.092	10	2	28	28	30	28	29	14	155
1138	0.11	20	2	11	11	11	11	11	6	50
1155	0.085	50	4	10	11	11	11	11	3	32

Table 38: Off-axis neutron dose equivalents for Linac C - 40 cm x 40 cm

Setup Parameters				Trial #	Distance [cm]		Collimator Setting		Temperature [°C]	
				1	100	SAD	40 cm x 40 cm		25	
Notes:	In air measurements, detector placed on treatment couch (only msd one side of iso to conserve sensitivity)			Accelerator			Energy		Date	
				Linac C			23 MV		9/29/2010	
Detector Number	Bubbles/ uSv	Detector Position [cm]	MU	Bubble Count				Bubbles Average	Bubbles /MU	uSv /MU
				1	2	3	4			
1201	0.1	0	2	37	41	40	38	39	20	195
1248	0.071	5	2	28	27	27	28	28	14	194
1150	0.092	10	2	34	33	34	33	34	17	182
1138	0.11	20	2	18	19	18	19	19	9	84
1155	0.085	50	4	10	11	10	11	11	3	31

Table 39: In water off-axis neutron dose equivalents for Linac L - 5 cm x 5 cm

Setup Parameters				Trial #	Distance [cm]		Collimator Setting		Temperature [°C]	
				2	100	SSD	5 cm x 5 cm		26	
Notes:	In water measurements, 3 cm depth			Accelerator			Energy		Date	
				Linac L			15 MV		10/9/2010	
Detector No.	Bubbles/ uSv	Off-Axis	MU	Bubble Count				Bubbles Average	Bubbles /MU	uSv /MU
				1	2	3	4			
1138	0.11	0	5	15	15	15	15	15	3	27
1201	0.1	5	5	11	11	11	11	11	2	22
1248	0.071	10	5	7	7	7	6	7	1	19
1150	0.092	15	5	7	7	7	7	7	1	15
1155	0.085	20	5	7	7	7	7	7	1	16

Table 40: In water off-axis neutron dose equivalents for Linac L - 10 cm x 10 cm

Setup Parameters				Trial #	Distance [cm]		Collimator Setting		Temperature [°C]	
				2	100	SSD	10 cm x 10 cm		26	
Notes:	In water measurements, 3 cm depth			Accelerator			Energy		Date	
				Linac L			15 MV		10/9/2010	
Detector No.	Bubbles/ uSv	Off-Axis	MU	Bubble Count				Bubbles Average	Bubbles /MU	uSv /MU
				1	2	3	4			
1248	0.071	0	5	14	14	14	14	14	3	39
1138	0.11	5	5	14	14	14	14	14	3	25
1201	0.1	10	5	9	9	9	9	9	2	18
1248	0.071	15	5	5	5	5	5	5	1	14
1155	0.085	20	5	8	8	8	8	8	2	19

Table 41: In water off-axis neutron dose equivalents for Linac L - 20 cm x 20 cm

Setup Parameters				Trial #	Distance [cm]		Collimator Setting		Temperature [°C]	
				2	100	SSD	20 cm x 20 cm		26	
Notes:	In water measurements, 3 cm depth			Accelerator			Energy		Date	
				Linac L			15 MV		10/9/2010	
Detector No.	Bubbles/ uSv	Off-Axis	MU	Bubble Count				Bubbles Average	Bubbles /MU	uSv /MU
				1	2	3	4			
1150	0.092	-15	10	16	15	15	15	15	2	17
1155	0.085	0	5	21	21	21	21	21	4	49
1248	0.071	5	5	12	12	12	12	12	2	34
1138	0.11	10	5	17	18	17	17	17	3	31
1201	0.1	15	10	18	18	18	18	18	2	18
1201	0.1	20	10	19	19	18	18	19	2	19

Table 42: In water off-axis neutron dose equivalents for Linac L - 40 cm x 40 cm

Setup Parameters				Trial #	Distance [cm]		Collimator Setting		Temperature [°C]	
				2	100	SSD	40 cm x 40 cm		26	
Notes:	In water measurements, 3 cm depth			Accelerator			Energy		Date	
				Linac L			15 MV		10/9/2010	
Detector No.	Bubbles/ uSv	Off-Axis	MU	Bubble Count				Bubbles Average	Bubbles /MU	uSv /MU
				1	2	3	4			
1248	0.071	0	5	19	19	19	19	19	4	54
1201	0.1	5	5	18	17	18	19	18	4	36
1155	0.085	10	5	14	14	14	14	14	3	33
1150	0.092	15	5	10	10	10	10	10	2	22
1150	0.092	20	5	9	9	10	9	9	2	20

Table 43: 15 MV neutron dose equivalents as a function of increasing depth in water for a 5 cm x 5 cm field

Setup Parameters				Trial #	Distance [cm]		Collimator Setting		Temperature [°C]	
				2	100	SSD	5 cm x 5 cm		26	
Notes:	In water measurements			Accelerator			Energy		Date	
				Linac L			15 MV		10/8/2010	
Detector No.	Bubbles /uSv	Detector Depth [cm]	MU	Bubble Count				Bubbles Average	Bubbles /MU	uSv /MU
				1	2	3	4			
1248	0.071	1	4	10	10	10	10	10	3	35
1138	0.11	5	5	15	15	15	15	15	3	27
1150	0.092	10	10	16	16	16	16	16	2	17
1201	0.1	15	15	22	22	22	22	22	1	15
1155	0.085	25	20	18	18	18	18	18	1	11

Table 44: 15 MV neutron dose equivalents as a function of increasing depth in water for a 10 cm x 10 cm field

Setup Parameters				Trial #	Distance [cm]		Collimator Setting		Temperature [°C]	
				1	100	SSD	10 cm x 10 cm		26	
Notes:	In water measurements			Accelerator			Energy		Date	
				Linac L			15 MV		10/8/2010	
Detector No.	Bubbles /uSv	Detector Depth [cm]	MU	Bubble Count				Bubbles Average	Bubbles /MU	uSv /MU
				1	2	3	4			
1201	0.1	1	5	23	23	23	23	23	5	46
1248	0.071	3	5	14	14	14	14	14	3	39
1248	0.071	4	5	13	13	13	13	13	3	37
1248	0.071	5	5	11	11	11	11	11	2	31
1201	0.1	10	20	39	43	40	40	41	2	20
1150	0.092	12	10	12	12	12	12	12	1	13
1150	0.092	15	10	11	11	11	11	11	1	12
1248	0.071	20	20	19	19	19	19	19	1	13
1201	0.1	25	10	12	12	12	11	12	1	12

Table 45: 15 MV neutron dose equivalents as a function of increasing depth in water for a 20 cm x 20 cm field

Setup Parameters				Trial #	Distance [cm]		Collimator Setting		Temperature [°C]	
				2	100	SSD	20 cm x 20 cm		26	
Notes:	In water measurements			Accelerator			Energy		Date	
				Linac L			15 MV		10/8/2010	
Detector No.	Bubbles /uSv	Detector Depth [cm]	MU	Bubble Count				Bubbles Average	Bubbles /MU	uSv /MU
				1	2	3	4			
1155	0.085	1	4	22	22	22	22	22	6	65
1201	0.1	5	5	19	19	19	19	19	4	38
1248	0.071	10	5	11	11	11	11	11	2	31
1201	0.1	15	10	14	14	14	14	14	1	14
1138	0.11	25	15	20	21	20	21	21	1	12

Table 46: 15 MV neutron dose equivalents as a function of increasing depth in water for a 40 cm x 40 cm field

Setup Parameters				Trial #	Distance [cm]		Collimator Setting		Temperature [°C]	
				2	100	SSD	40 cm x 40 cm		26	
Notes:	In water measurements			Accelerator			Energy		Date	
				Linac L			15 MV		10/8/2010	
Detector No.	Bubbles /uSv	Detector Depth [cm]	MU	Bubble Count				Bubbles Average	Bubbles /MU	uSv /MU
				1	2	3	4			
1150	0.092	1	4	25	25	25	25	25	6	68
1248	0.071	5	5	16	16	16	16	16	3	45
1138	0.11	10	10	26	26	26	26	26	3	24
1150	0.092	15	10	16	16	16	16	16	2	17
1138	0.11	25	15	17	17	17	17	17	1	10

Table 47: 23 MV neutron dose equivalents as a function of increasing depth in water for a 10 cm x 10 cm field

Setup Parameters				Trial #	Distance [cm]		Collimator Setting		Temperature [°C]	
				1	100	SSD	10 cm x 10 cm		26	
Notes:	In water measurements			Accelerator			Energy		Date	
				Linac C			23 MV		10/3/2010	
Detector No.	Bubbles/ uSv	Detector Depth [cm]	MU	Bubble Count				Bubbles Average	Bubbles /MU	uSv /MU
				1	2	3	4			
1150	0.092	3	2	32	30	30	30	31	15	166
1138	0.11	4	2	29	28	27	26	28	14	125
1150	0.092	5	2	16	16	14	16	16	8	84
1248	0.071	10	2	9	9	10	9	9	5	65
1201	0.1	15	2	11	11	11	11	11	6	55
1155	0.085	20	2	7	7	7	7	7	4	41
1248	0.071	22	2	5	5	4	4	5	2	32

Table 48: Raw results for a 10 cm x 10 cm field, 15 cm off-axis with detector shielded by 5 cm of BPE

Trial	SSD [cm]	depth [cm]	MU	Detector No.	Bubbles /uSv	1	2	3	4	avg	bubbles/ MU	uSv/ MU
1	90	10	50	1155	0.085	4	4	4	4	4	0.08	0.94
2	90	10	150	1150	0.092	14	14	15	14	14	0.10	1.03
3	90	10	150	1248	0.071	10	10	10	10	10	0.07	0.94

Table 49: Raw results for a 10 cm x 10 cm field, 15 cm off-axis with no BPE shielding

Trial	SSD [cm]	depth [cm]	MU	Detector No.	Bubbles /uSv	1	2	3	4	avg	bubbles/ MU	uSv/ MU
1	90	10	40	1248	0.071	12	12	12	12	12	0.30	4.23
2	90	10	40	1201	0.1	17	16	16	17	17	0.41	4.13
3	90	10	40	155	0.085	14	13	14	14	14	0.34	4.04

Table 50: IMRT Raw Results

Plan	SSD [cm]	depth [cm]	Detector No.	Bubbles/uSv	1	2	3	4	avg	uSv
1	90	10	10161248	0.071	27	28	27	28	28	387
2	90	10	10161201	0.1	36	35	34	34	35	348
3	90	10	10161150	0.092	37	36	37	36	37	397

BTI BUBBLE Technology Industries

Calibration Certificate

Temperature Compensated BD-PND Bubble Dosimeter(s)

Customer: Pulcir Incorporated **BTI Job No.:** 168

Customer Order No.: Gerger

Detector Type	Detector Number BD-PND	Average Sensitivity @ 20-37C Bubbles/mrem	Bubbles/uSv
BD-PND	10112228	32	3.0
BD-PND	10117135	30	2.8
BD-PND	10117148	33	3.0
BD-PND	10117215	31	2.9
BD-PND	10117224	30	2.8
BD-PND	10161138	1.2	0.11
BD-PND	10161150	0.98	0.092
BD-PND	10161155	0.91	0.085
BD-PND	10161201	1.1	0.10
BD-PND	10161248	0.76	0.071

Between uses, the detectors must be stored, tightly sealed, in their original aluminum containers. Proper storage prolongs detector life and insures optimum performance.

Optimum storage temperature is from 20C-30C (68F-86F)

BTI BUBBLE Technology Industries

Calibration Certificate

Temperature Compensated BD-PND Bubble Dosimeter(s)

Customer: Pulcir Incorporated **BTI Job No.:** 168

Customer Order No.: Gerger

Detector Type	Detector Number BD-PND	Average Sensitivity @ 20-37C Bubbles/mrem	Bubbles/uSv

Description of the Bubble Dosimeter:
Model: BD-PND
Temperature compensated in the range 20°C to 37°C.

Calibration Method:
BD-PNDs are calibrated to an Am-Be source (strength = 1.13×10^{7} n/s, fluence weighted average energy = 4.15 MeV). A conversion factor of 3.70×10^{-5} mrem/n.cm^{-2} for the Am-Be source is used (as calculated from dose equivalent defined in NCRP Report No.38).
The detectors are calibrated at a distance from the source and a time period that produces approximately 100-150 bubbles. The source and detectors are held in an upright position in a Styrofoam jig parallel to each other. The BD-PNDs are calibrated 5 times using the neutron source: 1 calibration at each of 20°C, 24°C, 28°C, 35°C, and 37°C. The standard deviation of the 5 calibrations is less than 20%. The response quoted in this certificate is the average response over the temperature range 20°C-37°C.

Calibration Verified by: Betty Lance — Sept 13/10
Betty Lance
Production Technician **Date**

Order Reviewed by: Matt Koslowsky — Sept 13/2010
Matthias Koslowsky
Quality Representative **Date**

Between uses, the detectors must be stored, tightly sealed, in their original aluminum containers. Proper storage prolongs detector life and insures optimum performance.
Optimum storage temperature is from 20C-30C (68F-86F)